Suspended microchannel resonators for Biosensing applications

Facoltà di Ingegneria Civile e Industriale

Corso di Laurea in Ingegneria Magistrale Biomedica

Relatore

Prof. Domenico Caputo

Correlatore

Prof. Guillermo Villanueva

Damien Maillard

Candidato

Maria Vittoria Fedele

Anno accademico 2019/2020

Contents

1 Abstract

A Suspended microchannel resonator (SMR) is composed by a hollow resonant structure containing embedded microfluidic channel.
This device allows to circumvent the viscous damping confining the fluid to the inside of the resonant beam.
The goal of this project is to optimize the device developed in A. de Pastina's PhD work. She created and fabricated a SMR containing a microfluidic channel with piezoelectric electrodes embedded. The final objective is to measure mechanical properties of cells, studying their mass and stiffness. The deviation of these mechanical properties is linked to some diseases, as for the cancer cells.
The use of this device, monitoring the advancement of specific disease, could be an alternative to surgical techniques. It allows also to reduce the time and the cost of the results and to personalize the cure, avoiding the use of an invasive approach.

This project focuses on the fabrication of the two components of this device: electrodes and channels. Each step of the fabrication will be explained motivating the choice of materials and equipment used. Several references to the prior fabrication will be done, to understand which progress will be realized.

Acknowledgments

In the last year at University during one lesson of the course "*Tecniche ed Apparecchiature Biomedicali*" of my prof. Domenico Caputo, I had the pleasure to meet Annalisa De Pastina. She was a PhD student at Lausanne's University, EPFL. She explained about her research work and the high quality of research facilities and the international atmosphere of EPFL. These meeting gave me a strong impact on my choice to go there for my Master Project.

I am very thankful to my Prof. Domenico Caputo for giving me the opportunity to go to EPFL to work on my Thesis project, following me from a distance with interest and support.

I am grateful to Prof. Guillermo Villanueva for having me in his Lab ANEMS (*Advanced Nano-Electro-Mechanical Systems*), for his constant availability and guiding me in every step.

I am very thankful to Damien Maillard for following me from the first day. He thought me many things with dedication and precision, supporting and motivated me during each step. Our several discussions about the design and fabrication of devices were enriching experiences, helping me to discover all the aspects of the subject.

I would also like to thank the ANEMS group for his availability and kindness, it is a fantastic group where each component has his own quality.

Finally, thanks to the CMi (Centre of Micronanotechnology) Staff for helping me in the cleanroom during the fabrication of the devices.

2 Introduction: State of Art

A cell is defined as a complex dynamic system and the inspection of mechanical properties provides information about its health [1].

In the case of cancer, mechanical properties of cells have been connected to metastatic progression: Cancer cells were found to be more compliant than their healthy counterparts and the increase in elasticity and deformability was connected to intensified invasiveness [2].

The most widely established technique to perform deformability measurements of single cells from tissue sections is Atomic Force Microscopy (AFM), which examines cancer cell through their elastic properties.

The instrument consists of a cantilever with a probe tip at its free end, which applies a force or deformation at a defined speed into the cell. In this case there is a laser-photodiode system to measure the deflection of the cantilever that is correlated to the tip indentation in the cell [3].

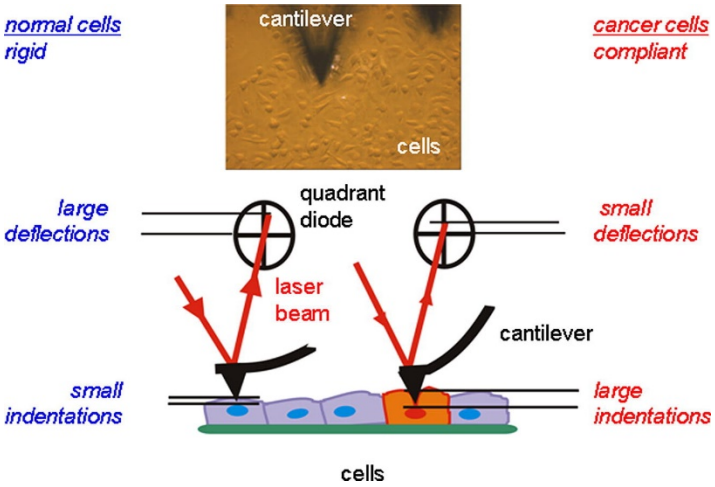

Figure 2.1: AFM measurements: for a normal cell the indentation depth is smaller (due to larger cell stiffness) resulting in larger deflections of the probing cantilevers; for a soft cell the depth is higher with a smaller cantilever deflection [3].

The cantilever is modelled as an elastic beam and its deflection is proportional to the force applied to the cell (Fig 2.1).

The formula describes the relation between the load force F and the resulting indentation depth δ :

$$F(\delta) = \frac{2 * \tan(\alpha)}{\pi * (1 - \mu_{cell})} * E_{cell} * \delta^2,$$

Where α is the open angle of the cantilever, μ_{cell} is the Poisson ratio related to the compressibility of the material (from 0 to 0,5). E_{cell} is the Young's modulus of the sample. The Young's modulus was used as an indicator of cell elasticity by doing a large number of measurements for different cells and in different locations due to the heterogeneity of cell structure [3]. The Young's modulus distributions were obtained from the Gaussian fit to all measurements and they showed significant differences between the distribution for normal cells and cancer cells (p=0.05), proving the lower ability to deform in the normal cells.

Wu and al. analysed and compared in detail a variety of different techniques developed for mechanical characterization of the rigidity and deformation of cells: AFM, magnetic twisting cytometry, parallel-plate rheometry and optical stretching. The optical stretcher allows to measure the stiffness of single cells with the use of a dual-beam optical trap inducing well-defined mechanical stresses on whole cells in suspension [4]. The value of the stiffness extracted in KPa varies by at least two orders of magnitude. For the optical stretcher the elasticity of a cancer cell was more than two orders of magnitude smaller than the elasticity measured by AFM: indeed the OS measures free-floating cells without rigid glass substrate.

A study of J. Tamayo and al. in 2015 demonstrated that MEMS resonant sensors, such as singly- and doubly-clamped microcantilevers, were an alternative to the traditional cell mechanical characterization methods. They used the resonant cantilevers to study the effect of the adsorption of the bacteria Escherichia coli on the resonance frequency [5]. They demonstrated that the frequency shift (magnitude and sign) depended on the position of the adsorbed bacterial cells. If the bacteria was deposited near the fixed region of the cantilever, the frequency increased. Since the resonance frequency shift should be negative with the addition of mass, the experiment meant that the surface stress strongly influenced the resonance frequency if the bacteria sticked near the clamp of the beam [5]. Another work of considerable importance was done by A. Corbin and co-workers., in which they used the resonant frequency to extract the mass and viscosity of cells added to their system.

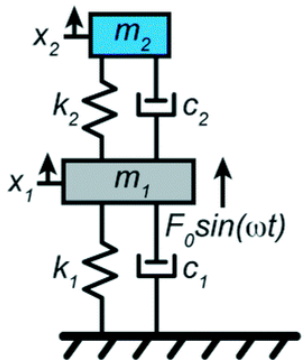

Figure 2.2: Free-body-diagram of the two-degree-of-freedom system model [3].

They modelled the cell behavior using a 2 DOF (Degree of Freedom) system, as depicted in Figure 2.2: the cell was represented as a Kelvin-Voigt viscoelastic material composed by a mass (m2) attached to a spring (k2) and damper (c2) in parallel. The cell was attached to the resonant sensor, a spring-mass-damper system itself (k1, m1, c1).[1]

They found a way to extract information about viscoelasticity removing the mass contribution: it can be obtained by an experimental fixation procedure. The resonant frequency was measured after making the object very stiff, like a fixation; in this way the amplitude of the frequency post and pre fixation can be used to know how soft cells are.

This work demonstrated that in cancer cells, Elastic moduli and viscosity values are lower than in benign cells, results validated with AFM [1].

2.1 Theory about Mechanical Resonators

Continuous advances in micro- and nanofabrication have driven the development of mechanical transducers with micro- and nanosized moving parts, such as membranes, beams or strings. Monitoring the characteristics of those devices allows to extract a variety of information, such as the mass and the stiffness of a cell. [6]

One-dimensional bending vibrations of beams are the principal nanomechanical structure used in research [7]. The studies of J. Tamayo on biosensors reported that the small size of these nanomechanical systems allows to reach a high sensitivity with respect to the mechanical properties of the adsorbed biomolecules. The displacement can be measured by optical and electrical techniques. The optical technique can be applied in vacuum or air or liquid: it consists of measuring the deflection of the laser beam reflected off the nanomechanical system surface with the use of a photodetector [6].

The piezoresistive technique is also an alternative method, integrating piezoresistive element on the clamping region.

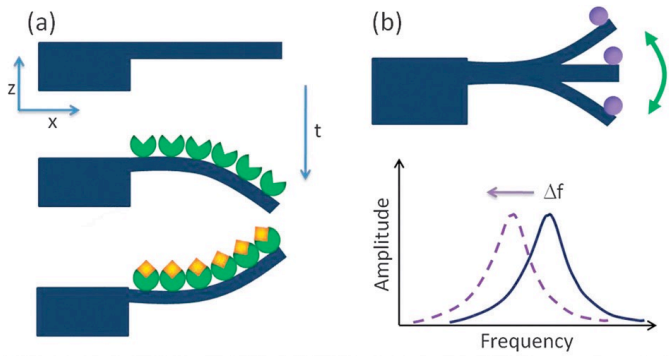

Figure 2.3: Main operation modes of nanomechanical biosensors: static mode (a) and dynamic mode (b). [6]

The nanomechanical biosensors could be classified in two classes, static and dynamic. In the static case (Figure 2.3a), the cantilever is functionalized with a monolayer of receptors. When the target molecules bind to the receptors, it creates a surface stress that can be characterized [8].

Dynamic mode biosensors are mechanical devices, characterized by a resonance frequency $f_r = \sqrt{\frac{k}{m}}$, proportional to the square root of the ratio between the effective stiffness and the effective mass of the device. When a biomolecule lands on the free end of the cantilever, there is a shift of the frequency, as depicted in Figure 2.3b [6,8,9].

To understand thoroughly the cantilever behavior, it is necessary to introduce the equation of motion given by Euler- Bernoulli [7]:

$$\rho A \frac{\partial^2 u(z,t)}{\partial t^2} + EI_z \frac{\partial^4 u(z,t)}{\partial z^4} = 0,$$

where u(z,t) is the displacement in the z-direction, ρ is the mass density, A the cross sectional area, E is Young's modulus and I_z is the geometric moment of inertia.

The solution of the Euler-Bernoulli equation is a harmonic that can be separated into a position-dependent and a time-dependent term:

$$U(z,t) = U_n(z)\exp(-i\omega_n t),$$

where n is the modal number and ω the frequency of motion.

With this solution the motion equation takes the following form:

$$-\rho A w^2 u(z,t) + EI\alpha^4{}_n u(z,t) = 0 \iff \omega = \alpha^2{}_n \sqrt{\frac{EI}{\rho A}},$$

where $\alpha_n = \frac{\lambda_n}{L}$ is the wavenumber associated to the n^{th} resonance mode, with λ_n equal to 1.1875 for the first mode of vibration.

The consequence of bimolecular adsorption is not only the change of the added mass but also of three other mechanical quantities: surface stress, stiffness, and viscoelasticity.

The study from Prof. San Paulo and co-workers unified all these quantities in a single equation:

$$\frac{\Delta f_r}{f_r} = \frac{3}{2}\frac{1}{\beta^4{}_n}\frac{d^2\Phi_n(x)^2}{dx^2}\frac{E_a}{E_b} - \frac{1}{2}\Phi^2{}_n(x)\frac{\rho_a}{\rho_b}\frac{V_a}{V_b},$$

where V is volume and the subscripts b and a denote the beam and adsorbate material, respectively; $\Phi(x)$ and $\frac{d^2\Phi_n(x)^2}{dx^2}$ are the amplitude of vibration and the curvature of the n^{th} vibration modes; E Young's modulus, ρ mass density.

In accordance to the Euler- Bernoulli beam theory, the resonance frequency of the n^{th} vibrational mode is calculated:

$$f_{r,n} = \frac{1}{2\pi}\sqrt{\frac{k}{m}},$$

with k and m the effective stiffness and mass, respectively [7].

From these equations, as reported before, it is clear that there exist two mechanisms that can produce an opposite effect on the frequency shift: the stiffness and the mass of the analytes, as it is explained in the following paragraph.

2.1.1 Responsivity and sensitivity

The change in resonant frequency due to a change in mass is called the Responsivity R of a resonant mass sensor [7].

$$R = \frac{\partial \mathrm{f}_r}{\partial m} \approx -\frac{1}{2}\frac{f_r}{m}$$

To obtain a high responsivity, a beam must have a high resonant frequency, by having low density and small dimensions. The sensitivity, that is the smallest detectable mass is approximately given by:

$$\Delta m_{min} = R^{-1}\Delta w_{min},$$

Where Δw_{min} is related to the noise of the system. To obtain a good resolution the noise should be reduced with a high Q-factor value, but it also depends by the condition of work and the scheme chosen.

2.1.2 Q-factor

A biological fluid exhibits both solid (elastic) and fluid (viscous) behavior. Tamayo affirmed that the mass sensitivity and frequency resolution are significantly degraded by the low-quality factor and large effective mass that is induced by viscous drag.

The quality factor (Q) of a mechanical resonator is defined as the ratio of stored energy over lost energy during one cycle of vibration [7]: for applications of micro- and nanomechanical resonators, a high Q is desired to improve the vibrational amplitude at resonance and reduce the resonance peak width. The dissipation is the inverse of the Q-factor and is the sum of different contributions, such as viscous damping, momentum exchange with the surrounding medium, or clamping losses [11]. The problem of damping and viscous drag associated with a resonant beam mass sensor in fluid can be circumvented by confining the fluid to the inside of the resonant beam while leaving the channel to operate in a gaseous environment or vacuum [9,12]. This technique has been developed by Burg and Manalis with devices called suspended microchannel resonators (SMRs) [12].

Clamping loss is one of the limiting damping effects, that is caused by radiation of vibrational energy through the anchor of the resonator. It can be important to choose the geometry of resonators in order to reduce clamping losses [7]. Silicon nitride material can be used to reduce this clamping problem: Q up to a million were demonstrated [13]. In this project the use of low stress Silicon Nitride (Is-SiNx) is essential to realize the channels as it will be explained in the Chapter 5.

2.1.3 Stiffness and vibration mode

In 2006, Tamayo affirmed that the frequency shift is function not only of the mass of the attached particles but also of the stiffness. For the fundamental vibration mode, the highest frequency responsivity to the added mass is achieved when the bacterial cells are located near the cantilever free end (the shift is negative). The best responsivity to the stiffness is observed near the clamp of the beam, due to the increase of the flexural rigidity (the shift is positive) [14].

These two behaviours are explained in Figure 2.4:

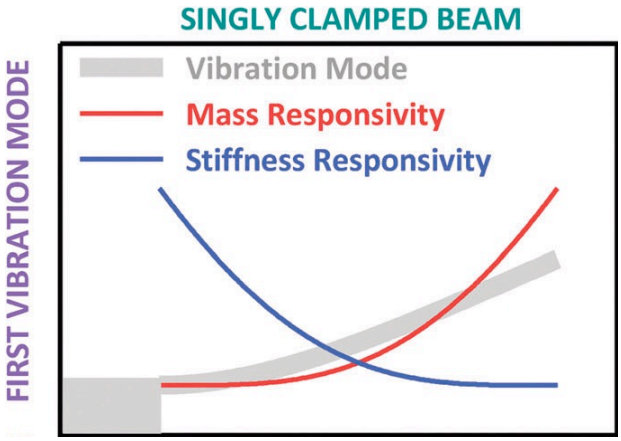

Figure 2.4: Resonance frequency responsivity to punctual changes of mass (red line) and stiffness (blue line) for singl-clamped beams for the first vibration mode.

Another research work by Tamayo, through the study of bacteria adsorption on the resonant frequency of a microcantilever, was useful to arrive at these conclusions: the relative resonant frequency shift of the flexural mode has the same behaviour of the torsional mode and his sign is independent of the number of cells utilized.

3 SMRs: Introduction

Suspended Microchannel Resonators (SMRs) are the best solution to minimize the problems previously described: they confine the analytes within the microfluidic channels embedded in themselves. The microcantilever deflection, in the first studies, was measured with a technique known as the optical-lever, an external component that was eliminated with the introduction of piezoresistive sensors: This allowed to integrate the electrical transduction on top of each channel, to measure the shift of the resonance frequency influenced by fluid mechanical properties.

3.1 Piezoelectric element

PZE materials are capable of converting mechanical energy into electrical energy and vice versa. This convertion is called “direct piezoelectric effect” and the opposite “converse piezoelectric effect”, Figure 3.1.

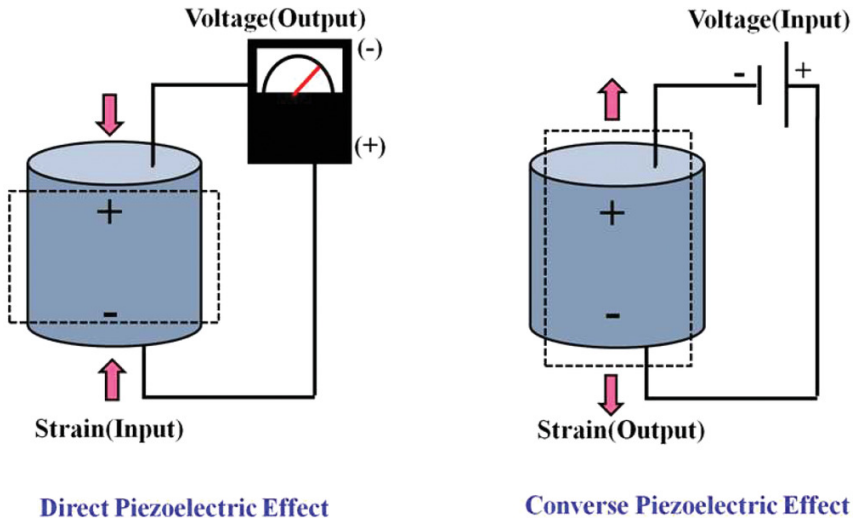

Figure 3.1: Dielectric Piezoelectric Effect and Converse Piezoelectric Effect

The coupling between the elastic and electric phenomena is described in this equation:

$$\varepsilon_i = C_{ij}\sigma_j + d_{ij}E_j$$

Where ε and σ are strain and stress vector, E the electric field, C the complaiance matrix and d the piezoelectric matrix.[7] In the crystalline structure, there is a balanced equilibrium between the positive and negative charges, and an application of mechanical stress resulted in a break of charge balance by destroying the neutrality of the molecule and thus creates a surface charge density that can be collected with electrodes.

Piezoelectricity is chosen as transduction not only for its intrinsic integrability, but also for the high efficiency, low power consumption, its non-dissipative effect and because it provides a fast and linear response. [8]

3.1 The Prior Art in the Lab

In the Prior Art developed by A. De Pastina [8] this kind of device was realized in order to enable the real time measurement of the fluid inside, and extract their mass and stiffness from the resonance frequency of the SMR, as shown in this figure:

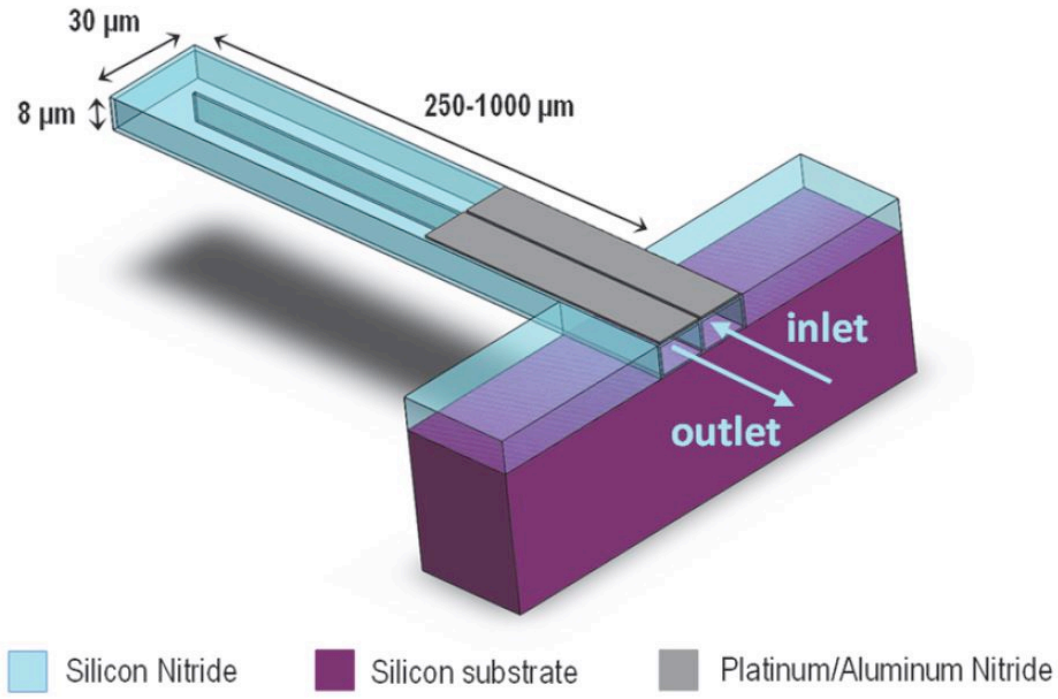

Figure 3.2: Schematic principle of the SMRs developed from Annalisa De Pastina

The device was realized in order to study the deformability of biological particles, like red blood cells (RBC), and to extract their mass and stiffness.

This device is equipped with piezoelectric transduction based on aluminium nitride (AlN): piezoelectricity has been used for both cantilever actuation and for the detection of the cantilever deflection.

The structural material for the channel is made of Low stress silicon nitride, for its transparency, biocompatibility and chemical stability [15], it will allow to see the analyte flowing inside the channel.

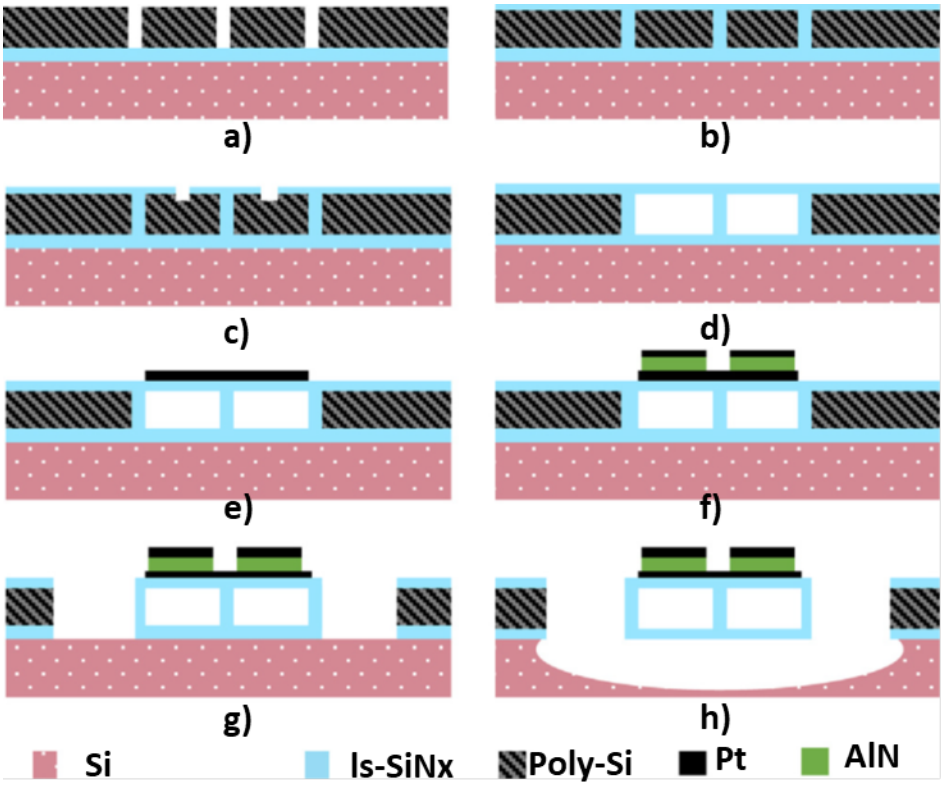

Figure 3.3: SMR fabrication process of A. De Pastina

The process flow developed is shows in Figure 3.3: 500 nm low stress silicon nitride (SiNx) and 6 um POCL3- doped PolySi are deposited on a 4-inch silicon wafer via low-pressure-chemical-vapor-deposition (LPCVD). The use of doped PolySi allows to reduce etching time during KOH procedure. The technique used to design the lateral walls of the fluidic channels is e-beam lithography. The channel is made by etching the silicon with the Bosch process (it will be explained in the following paragraphs) (a). Trenches are subsequently filled by a deposition of Is-SiNx (b). A c-C4F8-based dry etching defined the apertures on top of the fluidic channel, to provide access to the PolySi (c), emptied via KOH etching and sealed with 700 nm of Is-SiNx (d). For the bottom electrode 25 nm Platinum (Pt) is deposited at 300 °C and patterned (e), and for the top electrode, 300 nm Aluminium Nitride for the PZE active layer and 25nm Pt are sputtered at 300°C and patterned (f). SMRs are released, after an anisotropic dry etching used to define the resonator geometry, with a dry isotropic etching in SF6 gas (g,h).

3.2 The new fabrication method

The present work wants to optimize the complete fabrication process, with emphasis on the channels.

The principal issues in Annalisa's work were electrical losses due to the parasitic capacitance, in principle due to two factors: the large electrical tracks area, and for the use of Doped Polysilicon to realize the channels. For the electrodes the idea is to reduce the track area and limit as possible the overlapping between different tracks.

Regarding the channel fabrication, the channel will be etched directly into the silicon wafer, below a Is-SiNx membrane, to avoid the use of doped polysilicon.

Another important difference is the use of the Stepper for the Photolitography instead Ebeam lithography, it allows to reduce the process time and the difficulties of the fabrication. The discrepancies between these two procedures will be explained, in detail, in the Chapter 5.

4 Electrodes

As explained in the previous chapter the new idea is to reduce the track area and limit the overlapping between different tracks, in order to reduce parasitic capacitance and to gain a good insulation. Figure 4.1 compares the design done in the prior fabrication (a) and the new design (b): in both cases, the PZE tracks travel on separate paths and overlap only on top of the resonator, but in the new design the track area dimensions, and the overlapping area, are reduced.

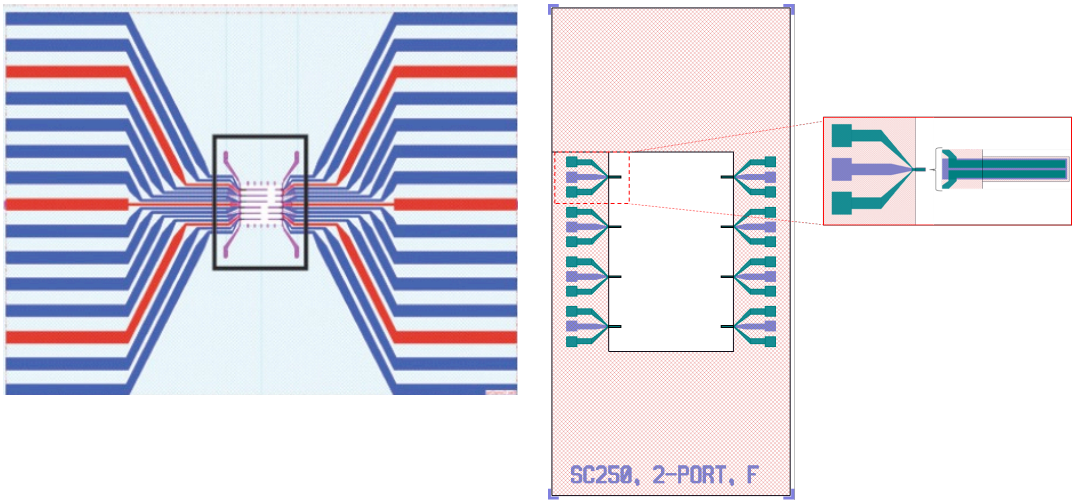

(a) (b)

Figure 4.1 Example of piezoelectric electrode design. (a) Prior design. (b) New design developed in this work.

The detailed process flow, with the exact parameters for each wafer, is attached in the Appendix A. Figure 4.2 shows a simplified cross section view with the different steps:

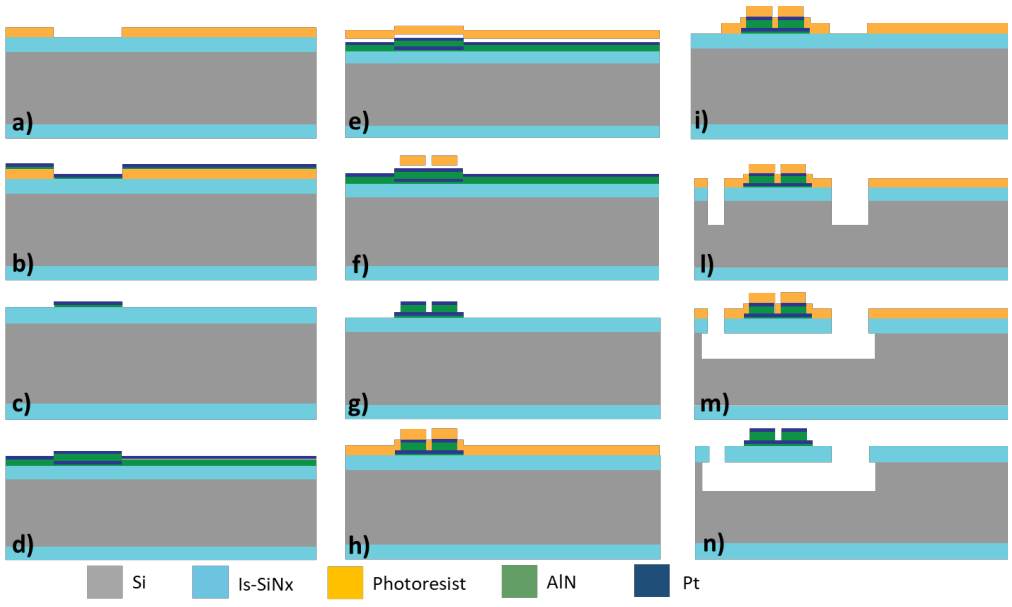

Figure 4.2: Electrodes Process Flow

The fabrication starts with a silicon wafer, 525um thick and 100mm in diameter. On this wafer a 500 nm thick layer of low stress silicon nitride (Is-SiNx) is deposited by CMI staff. The ls-SiNx acts as an efficient electrical insulator, his transparency is advantageous especially for the silicon substrate below the resonators during release [11].

The first step is the Photolithography of the bottom contact (a); layers of AlN and Pt is then sputtered on the substrate (b) and after that the bottom electrode is defined with the lift-off process (c); the AlN and Pt are subsequently sputtered for the piezoelectric (PZE) active layer and the top electrode (d); the process continues with another photolithography and an anisotropic dry etching defining the top contact (e,f,g); the last steps for the release are composed by a photolithography and two etching procedures, a Bosch process to define the resonators and an isotropic SF6 chemistry etching to release the device (h-n).

4.1 Design of electrodes

The design of the layout of a 4-inch Silicon wafer, was realized in CleWin 5, by Damien Maillard, a PhD student of the ANEMS lab in order to optimize the both the fabrication of the electrodes and their performance.

We define different mask layers: the first one represents the bottom electrode, the second the top electrodes and finally, the last one is the release. The layout contains 72 different Chips with different dimensions. There are some electrical test structures located in different regions to verify the insulation of AlN.

There are two chip configurations: they are either made with cantilevers or clamped-clamped beams. The simpler cantilever chip has got only one end of the beam clamped and it could be realized in two ways: two port or one port (Figure 4.3).

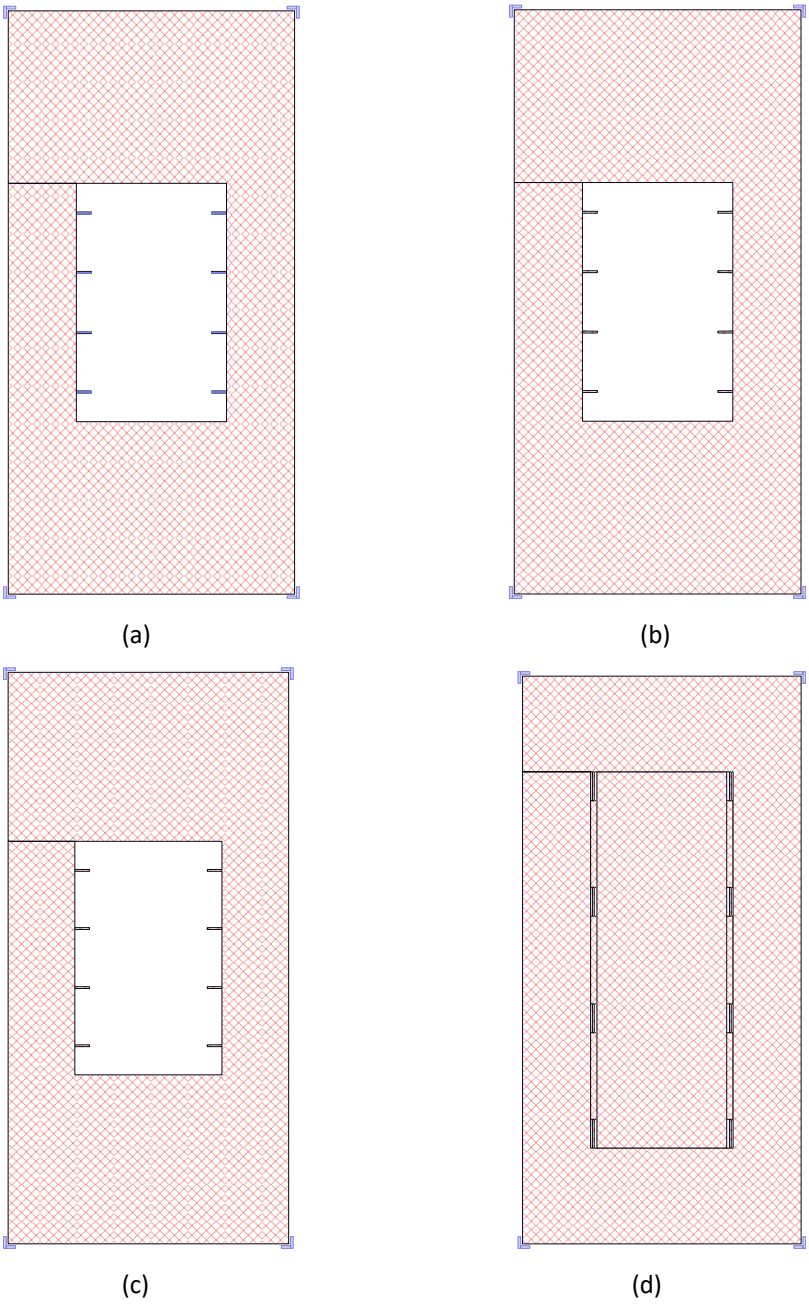

Figure 4.3 Simple cantilever design 250 um long: (a) Two port full length; (b) Two port 20% length ;(c) One port. (d) Double clamped beam design 500 um long.

In “two port” each resonator has two independent AlN/Pt fingers delivering actuation and readout signals: the beams are 50,100,250,500 um long and some electrodes extend for the total resonator length (Figure 4.3 a) and others extend for one fifth of the same length (Figure 4.3b, 4.4). This last

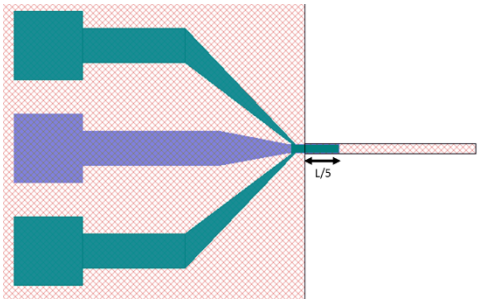

Figure 4.4 Electrodes extend for 1/5 of the total resonator length

choice allows to compare with A. De Pastina results [8], she used only this structure. We are changing the Bottom fabrication (the use of lift-off instead etching) and the path dimensions keeping the beam dimensions. We also test the longest because it is the best choice.

In “one port” there is only one electrode for the top to actuate and to detect, with the beams 50,100,250,500 um long.

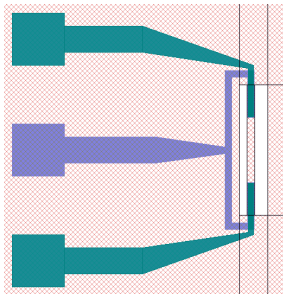

A doubly-clamped beam (Figure 4.3d, 4.5), is made of a single beam resonating at the centre with both ends fixed and the different beams are 250,500,750,1000 um long.

Figure 4.5 Double Clamped beam

The different designs with dimensions are reported in Table 4.1.

Design	Number of chips	Characteristics
Test Structure	14	• To check insulation of AlN • To check the conductivity
Simple Cantilever	24	• Two port L= (50,100, 250, 500 um) and 1/5 L • One port L= (50,100, 250, 500 um)
Double Cantilever	12	• L= 250, 500, 750, 1000 um

Table 4.1: Designs and dimensions of different chips of Electrodes

We realized five fabrications *(wafer numbers #38970, #38972, #38983, #85957, #85959)* with the same process flow but characterized by a different Active layer thickness (two wafers with 25nm, two wafers with 50nm, one wafer with 100nm).

4.2 Bottom Contact

The realization of the bottom contact is done with Lift off. It consists of exposing a pattern into photoresist, depositing a thin film over the entire area, then washing away the photoresist to leave the film only in the pattern area.

The wafer is coated with a 0.4um thick layer of LOR 5A, followed by 1.1 um positive photoresist AZ 1512, in the equipment *EVA150* [16]. The mask design is patterned over the wafer using the maskless aligner *MLA150*[17] by exposing the photoresist with a UV laser (405 nm) focused over the wafer with a dose of 50mJ/cm^2. The resolution has a minimum of about 1um, in this case the critical dimension is 5um.

The next step is the double development of the LOR and PR and deposition of the metal with the *SPIDER600* [18]. By experiences we know that the double development works better. We lose in dimensions, but it enables to avoid fences, redeposition of etching material during dry etching of Pt.

The *SPIDER600* allows metallic or insulating layers to be deposited on the wafer via sputtering, whose process is composed by four stages: the ions are generated by a plasma and directed towards the target, they pulverize the atoms of the target, the ejected atoms diffuse towards the substrate and part of the atomized atoms condense on the surface of the substrate to form a thin layer, as depicted in Figure 4.6.

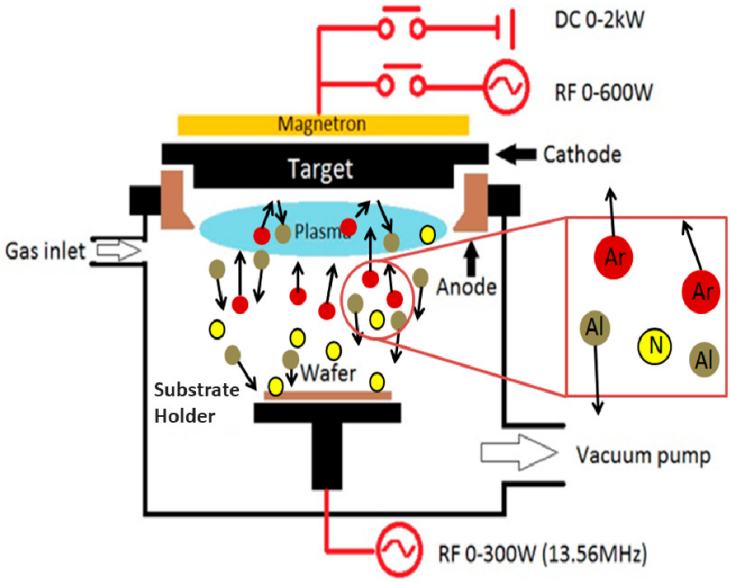

Figure 4.6: Description of sputtering

Before the deposition, the targets AlN and Pt need to be cleaned loading a dummy wafer.

After that the wafer is sputtered with 15 nm of AlN in one chamber, and with 25 nm of Pt in another chamber. The AlN layer is a “seed film” which limits residual stress, improving crystal orientation. The deposition parameters are reported in the Table 4.2.

Material	Recipe	Temperature	Gas flows [sccm]	Power[W]	Time
AlN clean	*AlN_clean*	RT	-	1500 W	-
Pt clean	*Pt_clean*	RT	5 (Ar)	500 W	-
AlN- 15 nm	*AlN_D1*	RT	40 (N2) 10 (Ar)	1500 W	18''
Pt- 25 nm	*Pt_D_Etch_D1*	RT	5 (Ar)	500 W	14''

Table 4.2 Deposition Active layer parameters

After the bottom contact deposition, the wafer is left in a bath of Remover 1165 overnight. The resist structures are removed together with the material deposited thereon, while the material applied directly to the substrate through the openings of the resist mask remains there as desired.

After the development and before lift-off the wafers are inspected with microscope to check the Resolution. Figures 4.7, 4.8 show two examples of bottom feature measured in comparison with the theoretical sizes of the same design.

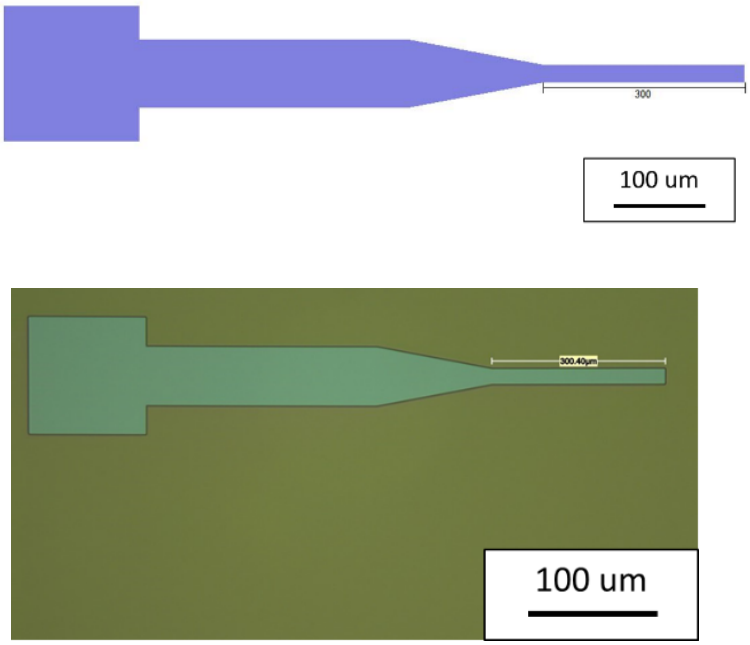

Figure 4.7: Bottom contact feature of a singly-clamped beam 250 um long. The length of the electrode is close to the design. Picture taken with an Optical microscope.(Wafer #38972)

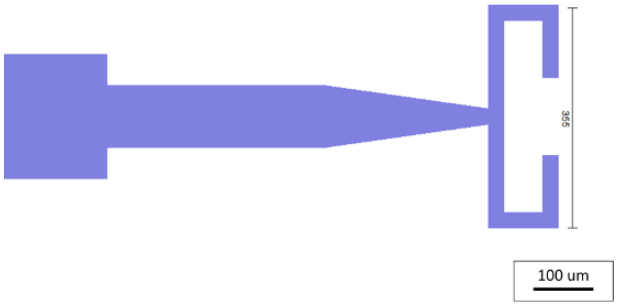

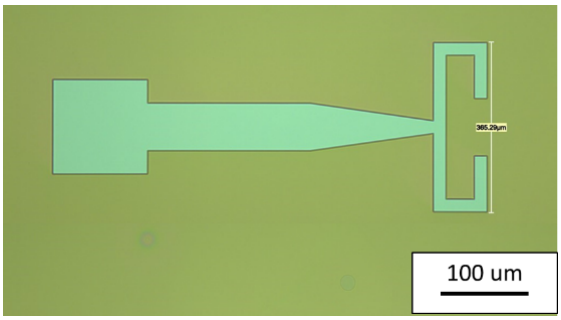

Figure 4.8: Bottom contact feature of a double clamped beam 250 um long. The length of the double clamped beam is close to the design. Picture taken with an Optical microscope. (Wafer #38983)

For this first deposition the dimensions in the wafers are close to the design dimensions. More attention will be paid after the deposition of the second and third layer to check the critical alignment.

4.3 Active Layer and Top Contact

The AlN is sputtered at 300°C for the active layer and 25 nm of Pt for the top electrode is deposited on top. During the deposition of AlN, it is critical to ensure that the reflective power is zero. If there is reflective power, not all the power is forwarded to the substrate, preventing a full control of AlN deposition and deteriorating the quality of the film.

Before the deposition, a test AlN deposition of 5 min is done on dummy wafer to check absence of reflecting power (RP=0). Active layer is realized with three different thickness: 100 nm,50 nm and 25 nm.

With an active layer thickness < 100 nm we gain a good electro-mechanical transduction and not too much added mass.

The deposition parameters are in Table 4.3.

Material	Recipe	Temperature	Gas flows [sccm]	Power[W]	Time
AlN clean	AlN_clean	300 °C	-	1500 W	-
Pt clean	Pt_clean	RT		500 W	-
RP check	AlN_T_D1	300 °C	40 (N2)	1500 W	5’
			10 (Ar)		
AlN	AlN_T_D1	300 °C	40 (N2)	1500 W	30’’ → 25nm
			10 (Ar)		1’ → 50nm
					2’ → 100nm
Pt- 25 nm	Pt_D_Etch_D1	RT	5 (Ar)	500 W	14’’

Table 4.2 Parameters for Deposition of Active layer

Cleland et al. confirmed the use of aluminium nitride as a piezoelectrical material for his stiffness with a Young’s modulus of 345 GPa, with a large piezoelectric constant e=1.5 C/m^2 and capacity to grow on single-crystal silicon.[19]

The wafer is then coated with a 1.5 um of positive resist AZ ECI 3007. The silicon is treated using Hexamethyldisilazane (HMDS) vapor before the coating, to gain a good adhesion of photoresist on inorganic materials.

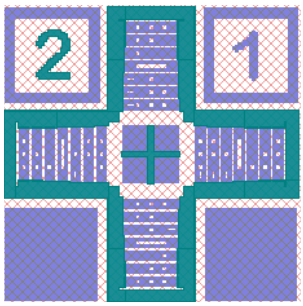

Figure 4.9: Alignment crossed from the first Layer and the second one

The equipment used for the coating and the following development is *ACS200* [20].

The Top electrode mask layer is aligned and inverted in the *MLA150* with the alignment crosses of the bottom metal (as shown in Figure 4.9), with a dose of 220mJ/cm^2. The inversion allows to expose where we don’t want the metal.

After the development it is important to have a look to the patterned photoresist with the Optical Microscope.

In Figure 4.10 it is shown the electrode with the beam 100um long. The two fingers representing the top contacts look centered with respect to the underlying bottom contact. The dimensions are very close to the design, Figure 4.11.

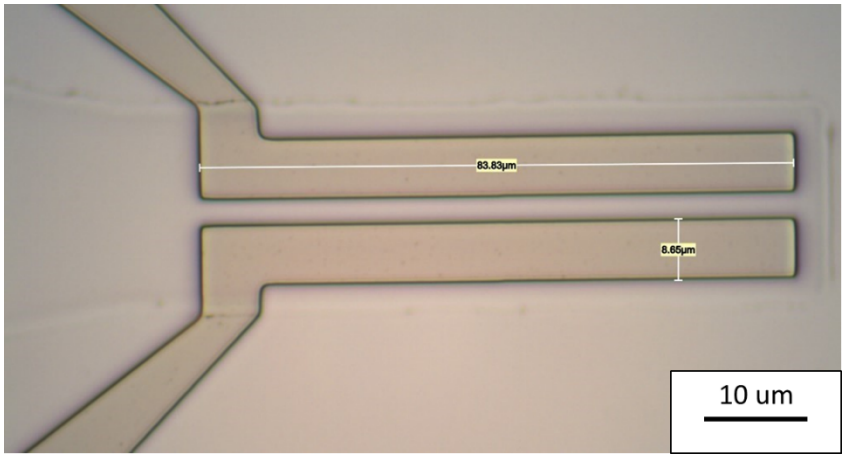

Figure 4.10: Features measurements of the top contact photoresist, the aligment looks respected. Wafer 38983 : Single clamped beam 100 um long.

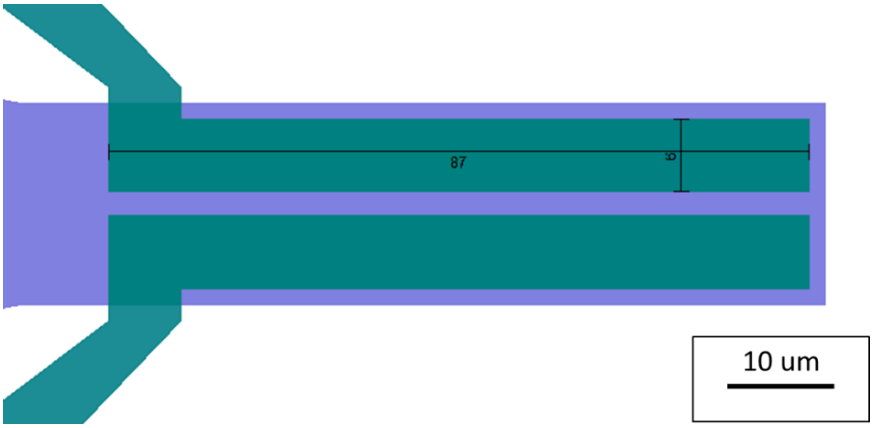

Figure 4.11: Theoretical features of the top electrodes as design in CleWin

The wafer is subsequently developed and dry etched by *STS Multiplex ICP* [21] (Inductively Coupled Plasma), in chlorine chemistry, using the Recipe "AlN_etch" to etch AlN and Pt in the areas not covered by the photoresist. In STS a Plasma is initiated with a radio-frequency magnetic field. In the chamber there are charges and ions and electrodes are deposited on the wafer, producing a negative potential. The positive ions descend toward the wafer, etching the surface. Two methods are used to determine if the etching is finished. The simpler is the eye-test: the colour of the bottom electrodes should be the same of the top. A second technique is the use of a multimeter in the bottom area to check if the metallic layer is removed.

Wafer 38983 is etched for 1'5''. Checking the Resistance between two points that are supposed to be insulated, there is a conductance. The possibility is that a thin layer of Pt is still on the wafer. The wafer is reloaded to continue the etching for 10''.

The photoresist is then stripped using *"Tepla Plasma Stipper"* [22] with high power Plasma for 3'. Plasma Etch is a gas-solid chemical reaction, an electrically neutral mixture of molecules, atoms, ions, electrons and photons. Another solution to strip the photoresist is the use of *"Ultrafab Wetbench"*: each wafer is placed for 5' in each of the two remover 1165 bath at 70°C. Then it is used a Quick Dump Rinse step following by a Cascade Tank (fine rinsing).

After these steps the use of the Probe Station is important in order to measure the electrical properties. It will be explained in Paragraph 4.5.

4.4 Release

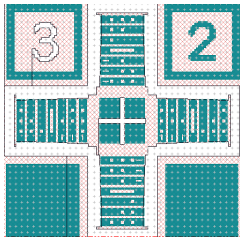

Figure 4.12: Alignment crossed from the release and top bottom

The last step of Electrode fabrication is the definition of single beam. A third photolithography was done at *ACS200*, using 4 um thick AZ9221 and HDMS. During the exposure with a dose of 225 mJ/cm^2 is important to invert the mask and use the alignment crosses from the top contact (Figure 4.12). The inversion allows to protect what is drawn, in this case I want to protect the cantilever.

Figure 4.13 compares the features sizes in a chip (wafer 38983) with a Singly-clamped beam "two-port" with the CleWin design. We see that the alignment of the photoresist area protecting the cantilever during the release in not well centred. The electrode is slightly closer to the top cantilever edges than to the bottom. This effect looks accentuated on the chips located in the edges of the wafer. This misalignment does not turn out to be problematic, because the electrode area is still well protected by the photoresist. Figure 4.14 depicts a simply-clamped beam but "one port", chip in the centre of the wafer 38983. We notice that in this case the misalignment is rather small.

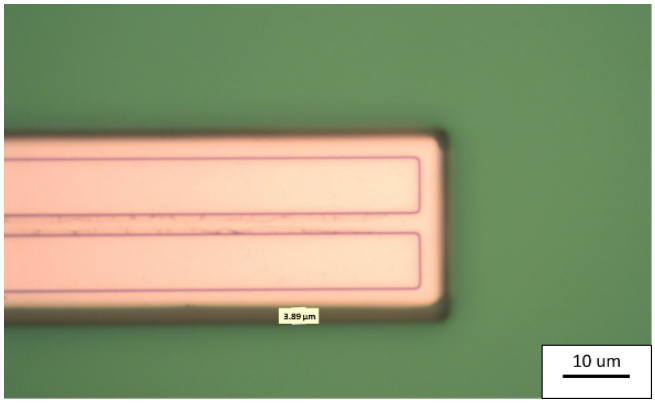

(a)

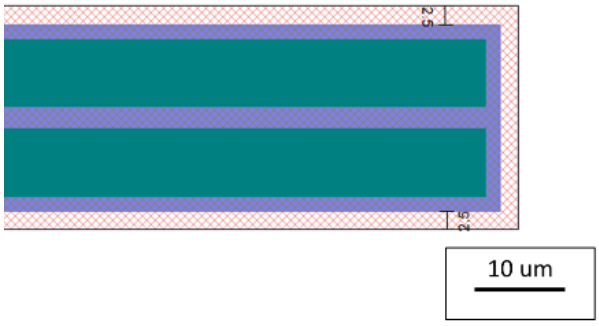

(b)

Figure 4.13: (a) Features measurements of the release photoresist for the wafer 38983: singly-clamped beam 100 um long. The misalignment is pronounced the electrode is closer to the top edge; (b) Theoretical features of the release photoresist in CleWin.

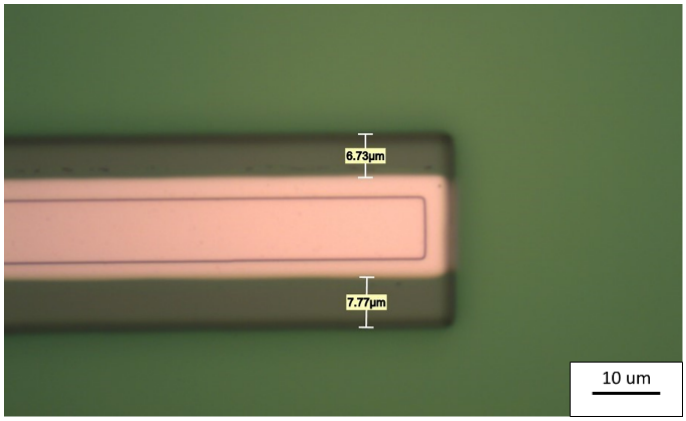

(a)

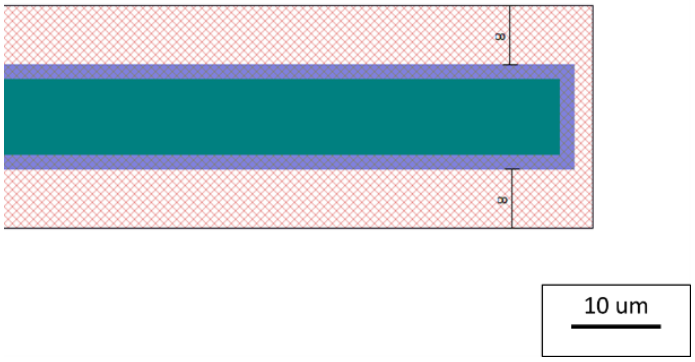

(b)

Figure 4.14: (a) Features measurements of the release photoresist for the wafer 38983: doubly-clamped beam 100 um long. The misalignment is rather small; (b) Theoretical features of the release photoresist in CleWin.

The process continues with the etching of Is-SiNx with the recipe "Si_smooth" for 2'50'' at *SPTS Advanced Plasma System* [23] that is an ICP-based high density plasma source, indeed it is difficult to etch dielectrics with the conventional ICP source.

A Bosch process step allows to etch down into the Si substrate with *AMS 200* [24]. Each cycle is composed by two steps: an anisotropic etching in sulfur hexafluoride SF6 and a passivation step in octafluorocyclobutane c-C4F8 to control lateral etch, as represented in figure 4.15. Thus, the etch step rapidly removes the polymer layer on the bottom of the feature while partially removing the polymer layer on the sidewall, allowing to etch anisotropically.

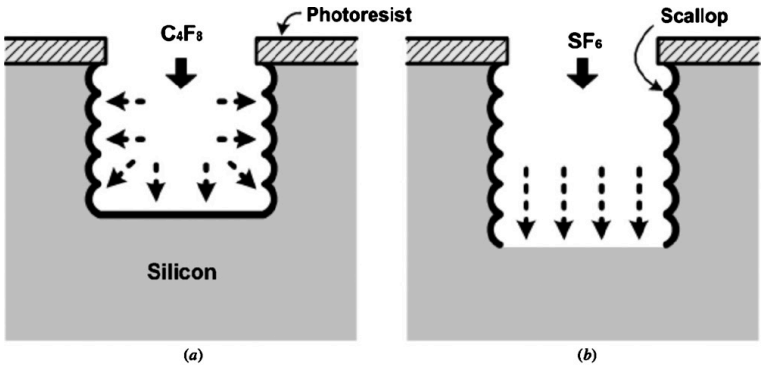

Figure 4.15: Bosch process: Passivation (a); Etching (b)

The recipes utilized for the Bosch process are "SOI_accurate--" for 12 cycles (10') later replaced by "SOI_accurate++++" for 6 cycles (1'), the specifications of each recipe are reported in the Table 4.4. For SF6 the flow rate is 300 sccm and for c-C4F8 150 sccm.

Recipe	SF6	C4F8
SOI_accurate----	5''	2''
SOI_accurate--	6''	2''
SOI_accurate+	6.5''	2''
SOI_accurate++	7''	2''
SOI_accurate++++	8''	2''

Table 4.4 Recipes for Bosch process

In this time-multiplexed process, the balance between etching and passivation is fundamental to gain anisotropic etching and process stability: if the etching step is fixed, an increase in C4F8 flow rate leads to an overall etch rate dropping. In addition to that, above an optimum value of C4F8 flow rate, where there is an ideal anisotropic etch rate, this one decreases sharply [25]. In this condition the etching pulse does not penetrate enough in the bottom polymer. For this reason, it is important to control not only the time value but also the flow rate to gain optimal isotropic etching results.

After completion of the Bosch process, another etching step is selected in the same equipment with a different recipe "Si_release" with only SF6, considering beam width of 30 um, a target of 15 um lateral is set.

Taking the advantage of the transparency of Is-SiNx, it is possible to see with an optical microscope a difference in color whether the underlying silicon was removed or not, having immediate confirmation of release completion.

On specifics, the first idea is to obtain a beam height of 40 um, by using the Bosch process for 10' with a cycle composed by 6'' of SF6 and 2'' of C4F8. Since the process is realized in only one step, by increasing the cantilever fragility, it is difficult to gain a successful suspension of the structure. After 9'30'' of "SOI_release", in steps, the device is inspected at first with the microscope, where it has been possible to understand that the release is incomplete (Fig 4.16a) and that 20 % of beams are broken especially for cantilever 500 um long like in Figure 4.16b. With SEM It is possible to find etching residues underneath the beam, due to the passivation layer, accumulated during the long Bosch process (Fig 4.16c, 4.16d).

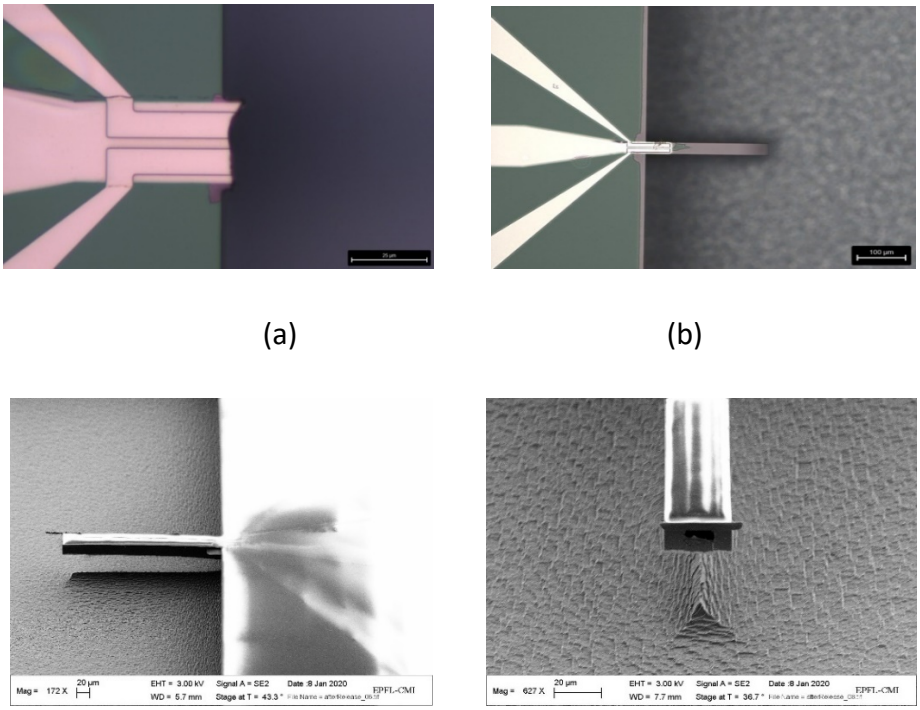

Figure 4.16: After Release: Microscope picture of a broken beam (a); Uncompleted etching after 9'30'' of Release(b); Residues of passivation accumulated during the long Bosch Process to etch trough the Si substrate (c) (d).

For all these reasons the following fabrications are realized with a reduced Bosch process time. The main difference is the choice to increase etching step time from 6'' to 8'' in each cycle; this allows to avoid having too much passivation residues.

To find the correct Bosch duration (reducing passivation residues and broken beams) the wafer is cleaved in four parts. In the first part, containing singly-clamped beams (250 um long) and doubly-clamped beams (250 um, 500 um, 750 um long), we use a Bosch process time of 1' and obtain a cavity depth of around 10 um. In the second part, containing singly-clamped beams, we run a 1'30'' long Bosch with the objective to increase the vertical distance, obtaining a beam highness of around 15 um. In Figure 4.17, an example of doubly-clamped beam after release is represented.

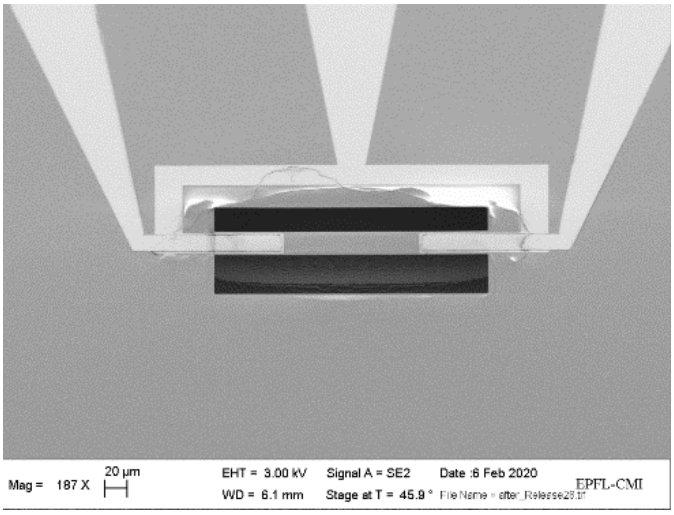

Figure 4.17 Douby-Clamped beam 500 um long, with a Bosch Procedure of 1'

4.5 Characterization

Each wafer, after the deposition of Active layer, is checked with the use of the Probe Station to study the conductivity of the metal and good insulation between top and bottom electrodes (R>MΩ). The probe station utilizes manipulators which allow the precise positioning of thin needle on the surface of the device.

In each wafer there are test structures located in different regions (edges and centre). The layout of a complete test structure is in Figure 4.18.

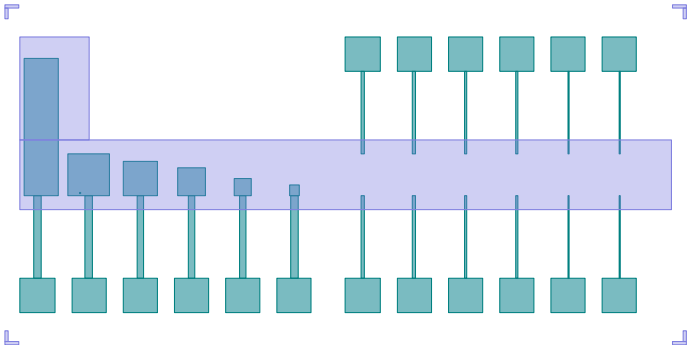

Figure 4.18: Layout of the test structure. The overlapping area between bottom and top electrodes increase.

We expect a lower Resistance between top and bottom Pt layer where the overlapping area is bigger, due to the greater chance to have not a good isolation.

The resistances measured between different pads on wafer *85959* are summarized in Graph of Figure 4.19.

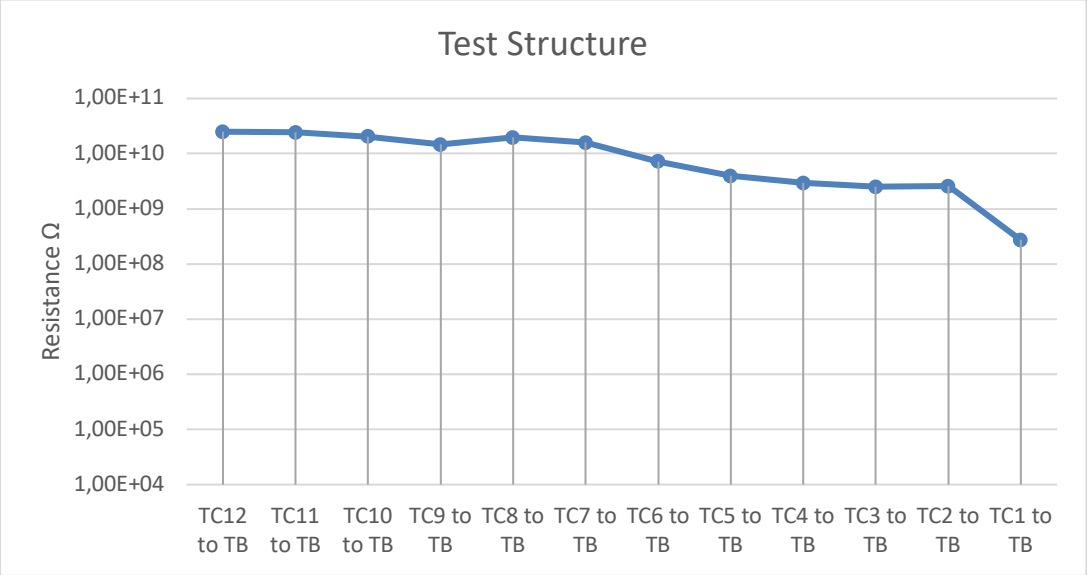

Figure 4.19: Resistance measured between different pas of the test structure of wafer 85989. The R has a value > 1 MΩ even changing the overlapping area.

The resistance between the top and bottom electrodes, ideally infinite, is measured with a voltage sweep from -0.5 to +0.5 V As we expected, the resistance is higher were the overlapping area is smaller. For this wafer we gain the best insulation the R reaches a maximum value of 2.5E+10 Ω without getting below the limit of 1MΩ.

For the wafer *85959* the insulation between bottom and top electrodes and the conductivity of the metal are checked in the 85% of the chips, with satisfactory results.

SC 50, 2-PORT F			
		Left	Right
Dev1	TC1-BC	1.97E+08	9.04E+07
	TC2-BC	6.96E+08	1.37E+09
	TC1-TC2	1.08E+09	1.62E+09
Dev2	TC1-BC	4.15E+08	2.98E+08
	TC2-BC	7.80E+08	1.03E+09
	TC1-TC2	1.47E+09	1.55E+09
Dev3	TC1-BC	7.01E+08	3.55E+08
	TC2-BC	6.96E+08	6.16E+08
	TC1-TC2	1.40E+09	1.22E+09
Dev4	TC1-BC	1.76E+08	2.50E+08
	TC2-BC	1.08E+06	1.50E+09
	TC1-TC2	1.80E+08	2.02E+09
bottToBott l°		21.9	
ToptoTop l°		12.68	

Table 4.5: Resistances measured between different pads of the chip Singly-clamped beam 50 um full length of wafer 85959. We notice a general satisfactory behavior for conductivity and insulation of the metal.

In Table 4.5 the chip singly-clamped beam 50 um full length is studied. We measure the insulation between top and bottom electrodes, obtaining an average resistance of 8.21E+08 MΩ > 1 MΩ.

For the wafer 38983 the resistance measured doesn't satisfy the required value; one reason could be the presence of AlN thin layer above the bottom electrode due to an under dry etching. In this case the resistance of the bottom was higher, as is depicted in Figure 4.20.

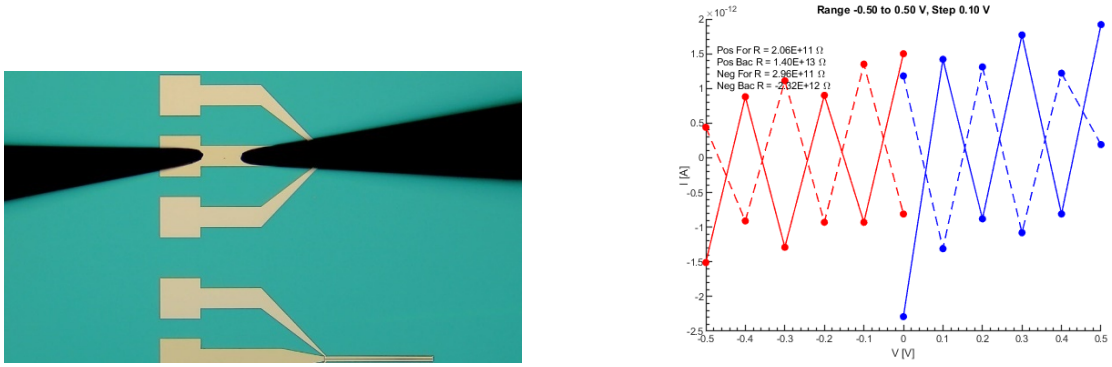

(a) (b)

Figure 4.20: (a) Probes placed on one bottom electrodes (b) Bad conductivity of the bottom electrode due to an insufficient dry etching of the AlN

It is possible to remove the excess AlN immersing the wafer in KOH etching and after a neutralization in HCl 37% for 2 hours. KOH etching is very aggressive for AlN, thus it is important to immerse the wafer only for a few seconds.

Fencing (resist and etched material) is another critical issue due to the redeposition of etching material during dry etching of Pt layers in chlorine chemistry, and it could short circuit PZE electrodes during the fabrication.

The cleaning of the etch equipment using a dummy wafer with the recipe "O2_clean", can help to avoid the deposition of other material during the etching process, on the side of the photoresist.

In principal we take two choices, the first one is the use of photoresist AZ ECI to avoid "straight wall" and the second one the use of the lift-off for the bottom layer.

Fences are inspected with a Scanning Electrode Microscope (SEM) that produces images of a sample by scanning the surface with a focused beam of electrodes (Figure 4.21).

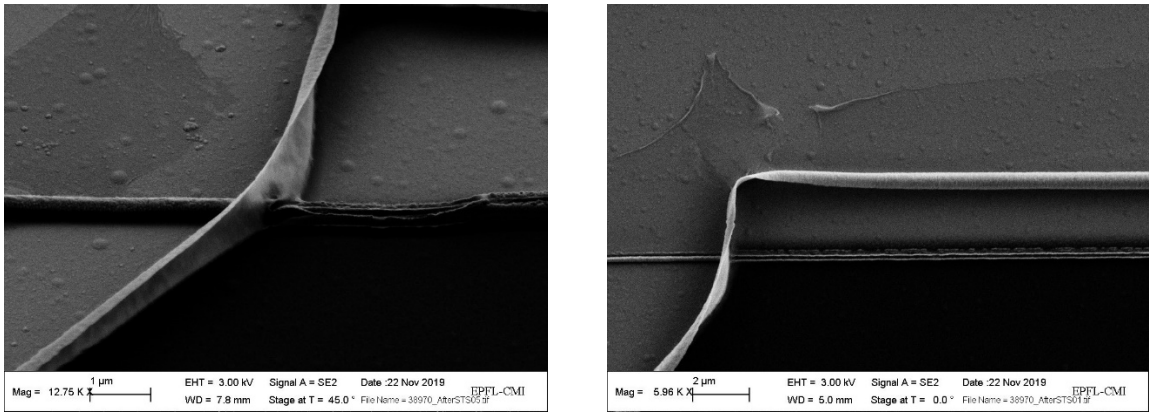

Figure 4.21: SEM pictures: Fences all around the pattern edge of the top electrodes in wafer 38970

As expected, the resistance value measured between different contact is lower than one MΩ. In figure 4.22 it is reported how the resistance behavior in the test structure.

The resistance is low not only for this chip but also for the chips located in each region of this wafer.

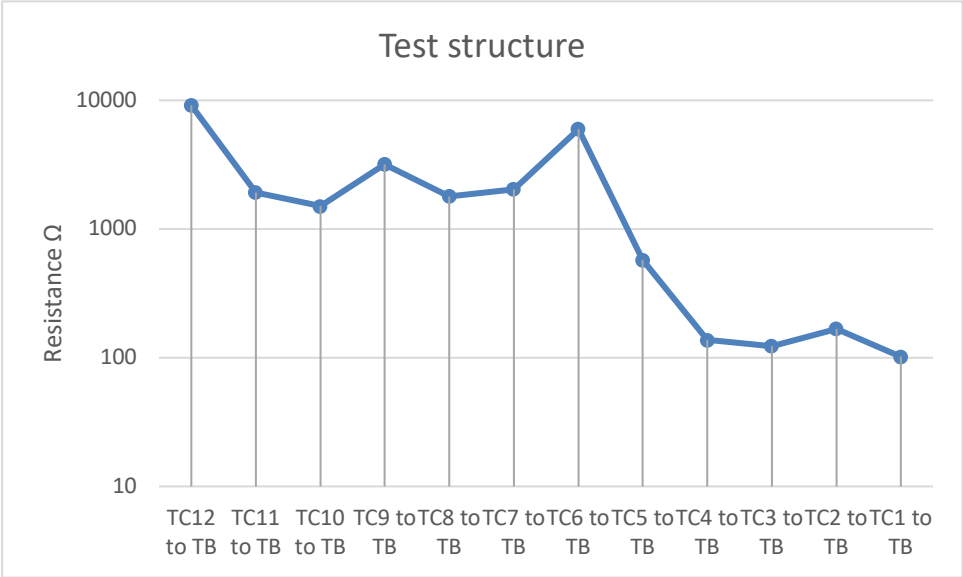

Figure 4.22: Test structure of the wafer 38970 with fences.

To study the PZE behavior we need to provide electrical connections. A simple PCB layout is developed and it is wire-bonded to the PZE electrodes pads on chip.

We used two different equipment to study the displacement of the PZE element: Laser Doppler Vibrometer (LDV) and Digital Holographic Microscope (DHM).

The LVD (OFV-551, Polytec GmbH) is used for the readout signal. For the actuation the Lock-in amplifier (UHFLI 600 MHz Boxcar Avarage, Zurich Instruments) generates the drive

voltage signal to the PCB for the chip. The LDV offers the displacement and velocity resolution making non invasive measurements. Figure 4.23 represents how a laser doppler work: the beam of the laser is split by a beam splitter (BS1) into a reference beam and a measurement beam. After passing through a second beam splitter (BS 2), the measurement beam is focused onto the sample which reflects it. This reflected beam is now deflected by BS2 and it is merged with the reference beam in the detector. The output signal modulated in frequency is directly proportional to the velocity and displacement of the sample. That value is converted in a voltage signal and fed to the lock-in amplifier. The conversional factor for the deflection of the resonator is equal to 50 nm/V.

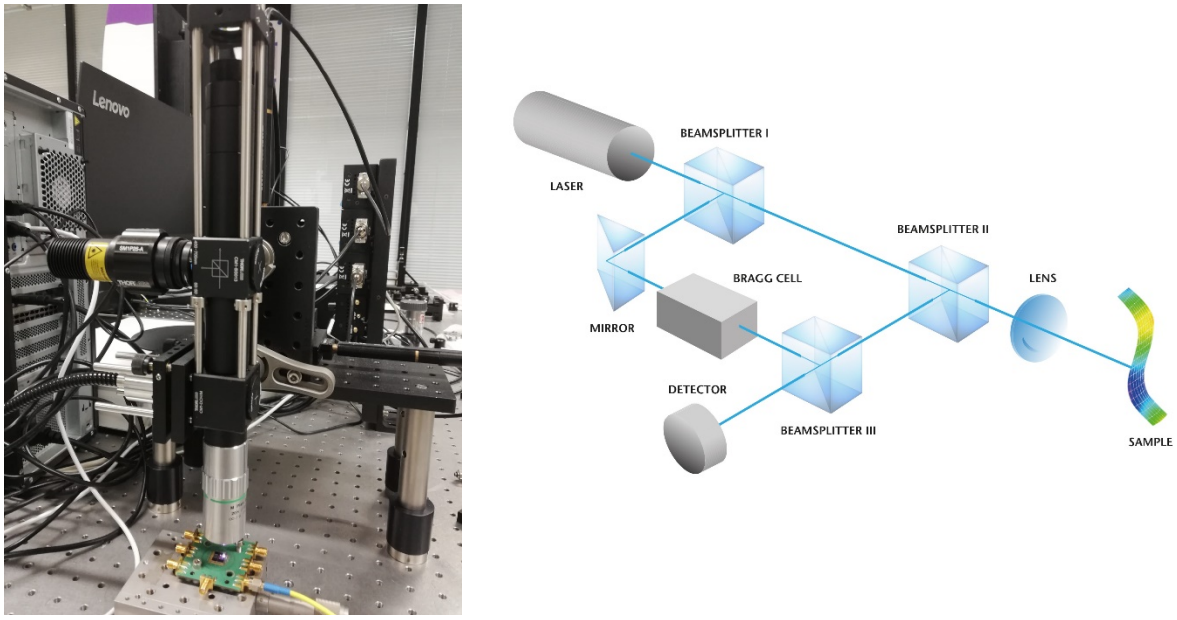

Figure 4.23: Measurement setup for electrode characterization in air. The chip is mounted on a PSB. In the first figure there is the microscope used to focus the LDV lase spot on top of resonators and provide optical red out. the second figure explains how a LDV works.

The DHM®-R2100 (Lyncée Tec) systems are based on a new technology allowing high frequency measurements at interferometric resolution. It captures holograms instead of intensity images as do conventional microscopes. The holograms are digitally interpreted using the Koala software supplied with the system to reconstruct an image of intensity and another of phase.

The principle of a DHM operating in reflection configuration is illustrated in figure 4.24.

The collimated source beam is separated in two: the object beam O and the reference beam R.

The retro diffused beam is collected by the objective of the microscope then recombined with the reference beam to form a hologram in the camera.

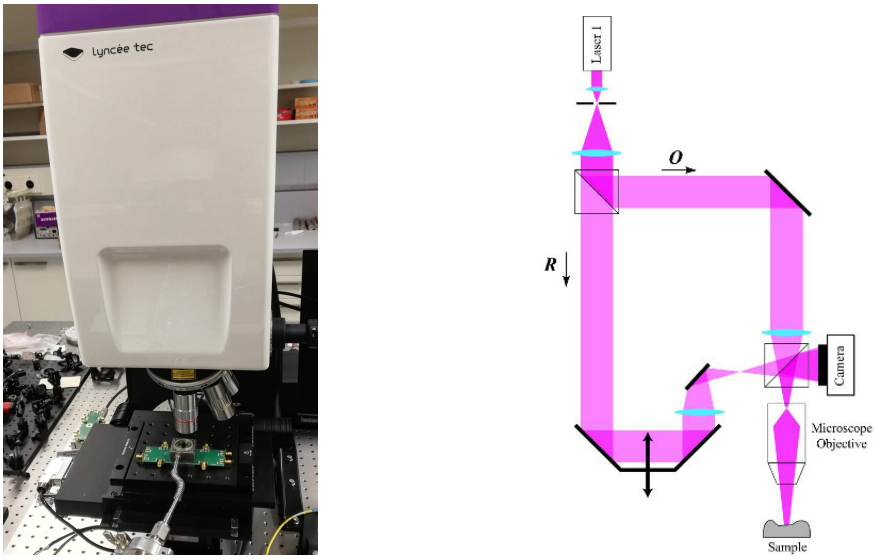

Figure 4.24 Single wavelength configuration

The R2100 DHM, allows to make alternative Dual Wavelength measurements, record two holograms. This DHM is equipped with an acquisition rate camera to work in stroboscopic mode. There is a synchronization between the movement of the sample, image acquisition and the illumination.

The chip analysed with these two equipments is the singly-clamped beam 50 um full length. In the chip four electrodes are wire-bonded to find the resonance frequency, the displacement at this frequency for different voltage in input.

Figure 4.25 presents the mechanical response, in air environment, as a function of the actuation voltage (50 mV). The resonance frequency and the quality factor were extracted from the Lorentzian fit. The frequency mean value is $153.8 \mp 0.026\ kHz$ and the Q-factor mean is 98.48 ∓ 3.17.

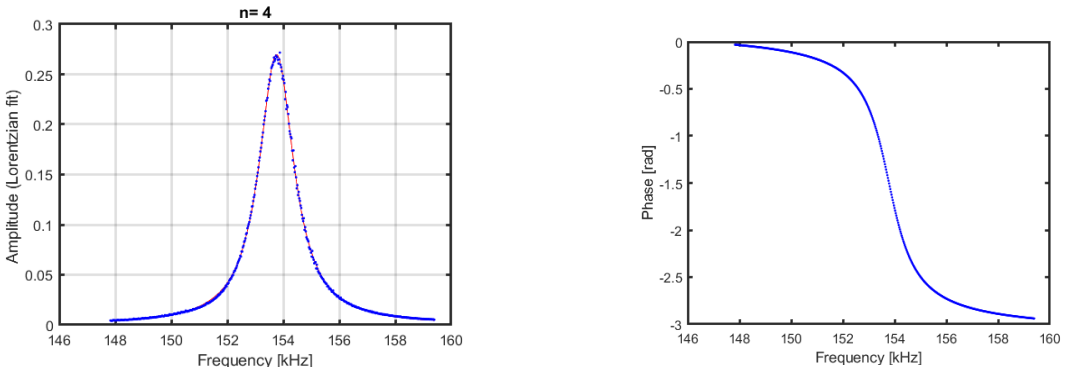

Figure 5.25: Mechanical response of a 50 um-long electrode, in air environment, as a function of the actuation voltage 50 mV.

The resonance frequency value is lower than the simulation value, equal to 299.4 KHz. A reason could be that the part released is longer than the cantilever length, it behaves like a longer beam. Figure 5.26 depicts the mechanical response of the same device as a function of different actuation voltage values. As expected from theory there is a linear relation between cantilever deflection and driving voltage.

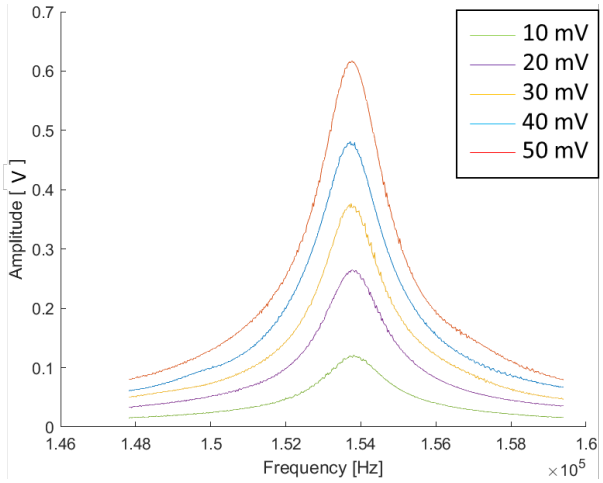

Figure 5.26: Amplitude for several actuations voltage: Linear behavior

The resonance frequency value is confirmed with the use of DHM. The dynamic analysis with the stroboscopic mode allows to acquire sequences of holograms to study the displacement at different input voltages, as depicted in Figure 5.27.

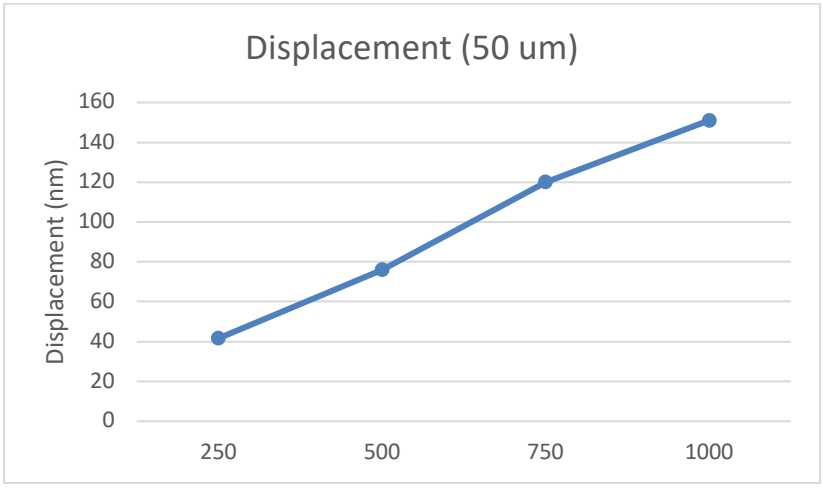

Figure 5.27: Displacement for different actuation voltage values

4.7 Chapter Conclusions

The fabrication of PZE suspended Electrodes is achieved with a process flow of 22 steps on a Si wafer covered by a substrate of Is-SiNx 500nm thick, where singly- and doubly-clamped beam, are designed and fabricated.

The piezoelectric layer is composed of Aluminium Nitride, which is deposited by sputtering at high temperature (300°C). We deposited different thicknesses: 25, 50 and 100 nm. Two-port devices enable independent actuation and readout of each cantilever. Bottom and top contacts are patterned with two different masks which are aligned with each other.

Fences are a major cause of short circuit, formed during dry etching, care must be taken to the cleaning of the equipment used (STS) and on the correct choice of photoresist.

The last photolithography defines the release to have the suspension of each beam. The suspension of beams is realized with the Bosch Process and different results have been achieved optimizing the process parameters and using the Is-SiNx transparency. We have gone from a vertical depth of 40 um to 20 um to avoid beam broken and passivation residues underneath.

The characterization of electrodes gives information about their electrical and mechanical performances.

The use of the probe station allows to check the conductivity and insulation. Fencing, due to a redeposition of etching material during the etching of Pt layer, causes short circuit of electrodes. We took two choices to reduce their presence: the use of the lift-off for the bottom electrode and of specific photoresist (AZ ECI) for the top layer.

The resonance frequency is found focusing the LDV laser at the tip of cantilevers, and with the DHM it is possible to calculate the displacement for different actuation voltage values.

5 Channels

The new micro-channels fabrication method developed, as explained in the third Chapter, has a main difference from A. De Pastina 's work [8]: to avoid the use of sacrificial material, thus etching directly in the silicon substrate. On top of the Silicon channel, a low-stress silicon nitride (Is-SiNx) layer is patterned with apertures, through which the channel is formed.

This new idea was previously applied in Zoé Daguin's Master Project [26], but instead of Ebeam lithography the present fabrication exploits the performance of Stepper. It allows to save tremendous amount of time. Additionally, it eliminates the need of a hard mask to protect the structures during fabrication.

The purpose of this work is to optimize and define the channel's features: membrane characteristics and minimum wall thickness between two channels. The design analysis will explain all the different variations in detail. The entire fabrication is reported in Appendix B. The Figure 5.1 explains the steps of the new process flow:

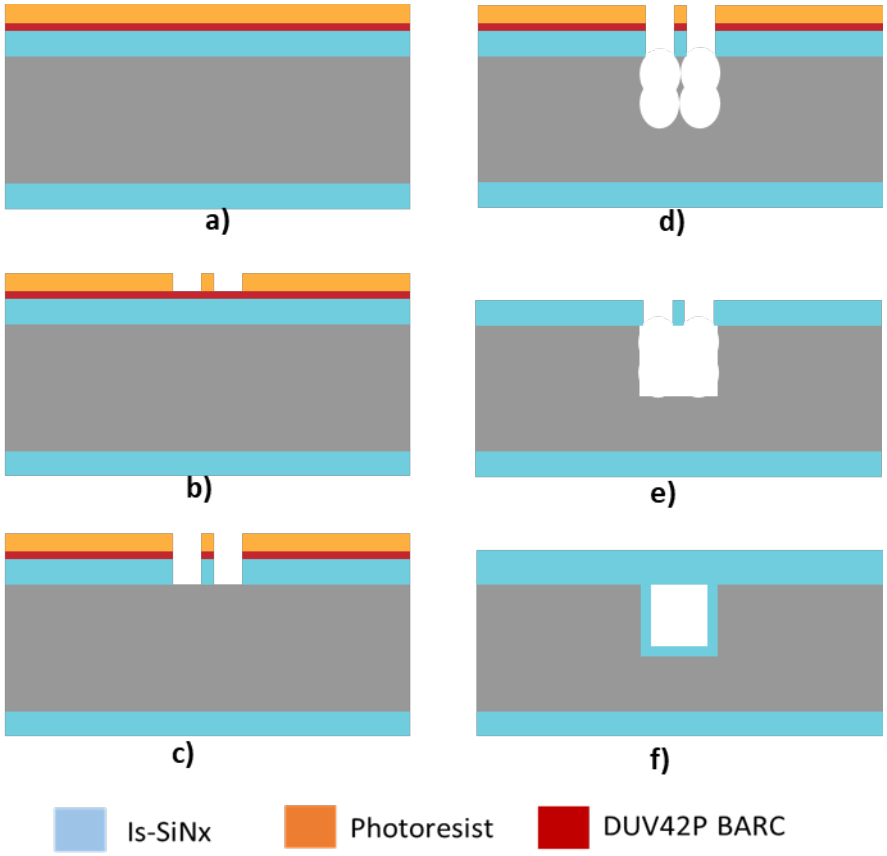

Figure 5.1: Process Flow: Channels

The fabrication starts with a silicon test wafer, with a 200 nm thick layer of low stress silicon nitride deposited by CMi staff. DUV42P BARC (Bottom Anti Reflective Coating) and a DUV resist (JSR M108Y (470 nm) or JSR M35G (1.2 um)) are coated (b), exposed in the Stepper and developed (b).

A dry etching step removes the BARC and the Is-SiNx until the silicon is reached (c). This realizes the nitride membrane below which the channel will be made. Vertical holes are etched by Bosch process (d). To remove the etching residues, a KOH 40% etching is utilized and a neutralization for two hours in HCl 37% follows (e). Then, RCA cleaning is done by CMi staff and afterwards, the deposition of low stress silicon nitride, 250 nm thick, to close the apertures.

5.2 Design

The design, started in Z. Daguin Master Project and completed in this work, is composed of three parts: "*Test structure-Channels*" to define and optimize the channel's membrane characteristics and the wall thickness, "*Test structure-Pillars*" to test membrane's robustness and at the end the "*TS structure-Device*" to try some full device expositions.

The design is sent to a fabricator (Toppan photomask, France) who realizes a Reticle industry standard 6''x6''x0.25'' quartz (ultra-low thermal-expansion) Cr blanks, used during the exposure.

The aperture sizes in the membrane need a clarification: during the mask fabrication with the use of the laser for the exposure and also with the following wet (isotropic) etching, all features are going to become wider. As such, we are going to lose 100nm per side. Additionally, and during the wafer realization, the etching of "BARC" will make everything 50 nm bigger per side. For this reason the apertures should be 300 nm smaller than the current value and the gap should be 300 nm bigger to keep the same pitch.

The dimensions used in this design refer to the Reticle and the wafer's dimensions will be reduced with a standard factor 4X. During the exposure with the Stepper the Reticle is not placed in contact with the wafer, like a mask-aligner, but there are projection lenses inserted between the Reticle and the wafer in order to reduce the image.

During the Design description, in this chapter, the dimensions refer to the wafer sizes.

5.2.1 Test Structure-Channels

Test structures are first fabricated to study the etching outcomes which means to define the correct size of membrane apertures, gaps between two adjacent squares, the corrections for the aperture edges and the wall thickness between two channels. There are six typologies of test structures (TS0, TS1, TS2, TS3, TS4 and TS5) that are disposed in arrays 2 cm long, with different corrections to try to obtain features as square as possible (the reason why we are using squared apertures will be explained in the Paragraph 5.3.3). All the design correction we attempted are represented in Figure 5.2 : the differences are the sizes and the number of squares placed in the corners. The first test structure TS0 is without correction, TS1 has a square in the corner with 0.2um side length, in TS2 and TS3 there is the same structure of before but the additional squares are 0.4 um and 0.6um, in TS4 a corner has three squares with 0.4 side length and TS5 is without correction (like TS0) but the side of apertures is 200 nm smaller. During the fabrication, inspecting the structures with SEM, it will be possible to evaluate the best design.

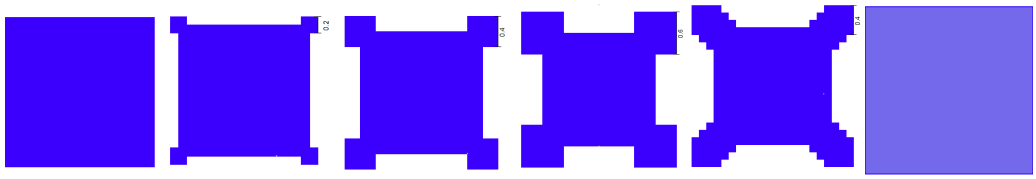

(a) (b) (c) (d) (e) (f)

Figure 5.2: TS0 without correction(a); TS1 one square l=0.2 (b); TS2 one square l=0.4(c);TS3 square l=0.6(d); TS4 three squares l=0.4 (e); TS5 without correction (f).

Each test structure is organized in two different patterns of two gap values (250 or 200 nm), that, in turn, are divided in four different arrays of distinct size apertures (600, 500, 400, 300 nm). Each array is composed of four identical lines, and spaced by 2 um, 1.5 um, 1 um to investigate the minimum distance between the channels. Figure 5.3 depicts TS4 composed by aperture size equal to 400 nm and gap value of 250 nm.

In the Table 5.1, we report the design dimensions for test structure TS4 (it resulted to be the best choice during fabrication, as it will be explained subsequently). We list the width of the line of each size aperture and the number of rows.

TS4-gap200	S 300	w=9.8 um	18 squares
	S 400	w=9.65um	15 squares
	S 500	w=9.65um	13 squares
	S 600	w=9.25um	11 squares
TS4-gap250	S 300	w=9.96um	20 squares
	S 400	w=9.55um	16 squares
	S 500	w=9.75um	14 squares
	S 600	w=9.55um	12 squares

Table 5.1: Characteristics of TS4: S=size of squares, w= width of channels

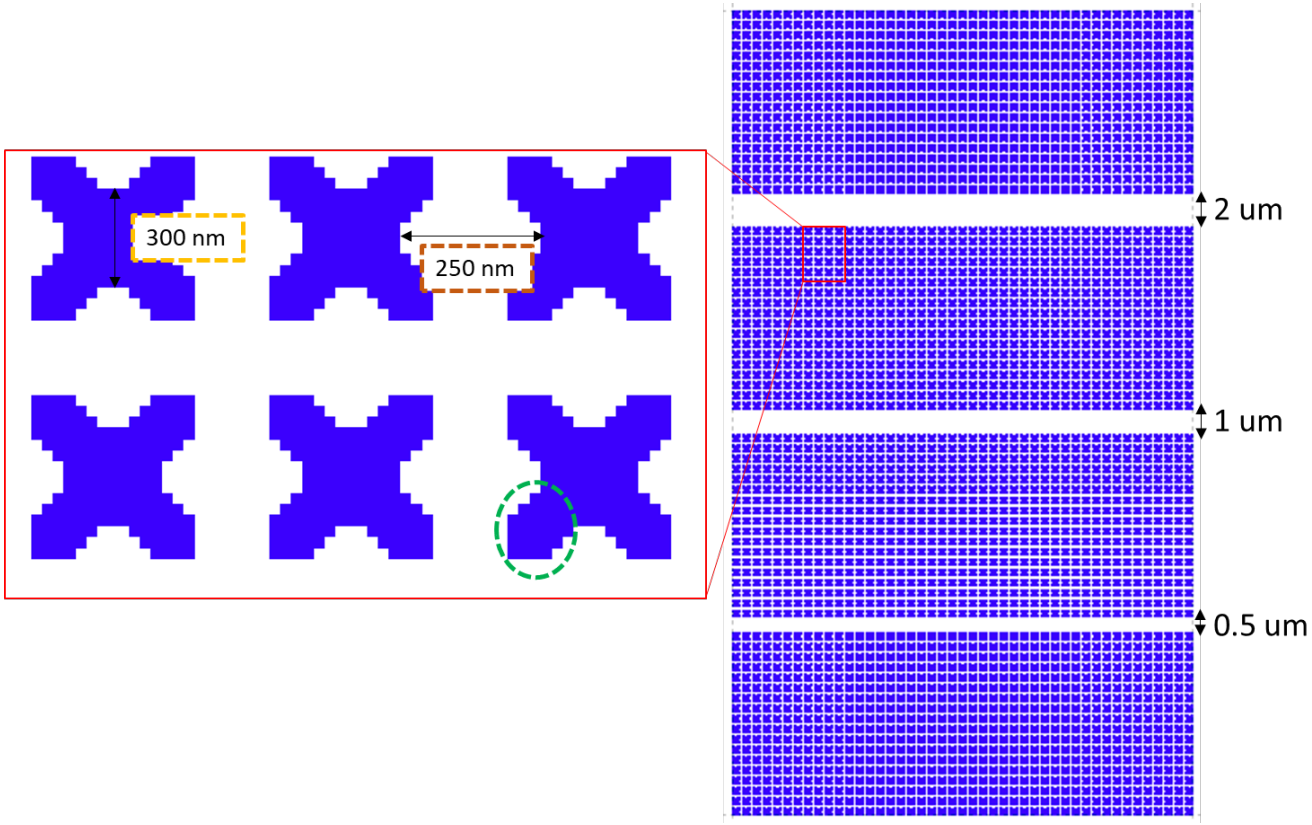

Figure 5.3: Example of TS4 with an aperture size 300nm and gap value 250nm, composed of four lines with different distances from each;

5.2.2 Test structure- Pillars

The suspended membrane is very fragile, especially if it becomes too large, and it can break. To give support to the membrane, pillars are used, made by removing some of the apertures (1X1,2X2,3X3,4X4,5X5 n° of apertures) and changing the period, i.e. the distance

between each of them (d= 10,20,30 um). An example is reported in Figure 5.4, where the pillars are made removing 3X3 apertures and have a period of 10 um.

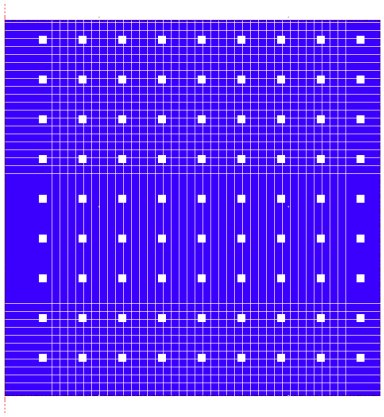

Figure 5.4: Test structure with pillars made by removing 3X3 and a period of 10 um

5.3 Fabrication

5.3.1 Photolithography

For the Photolithography we use the *ASML PAS DUV STEPPER*.

Bottom anti-reflection coating (BARC) and Deep Ultra Violet (DUV) photoresist layer are spin-coated and developed on *ACS200*. In the first fabrications, two resists are used: JSR Micro M108Y (470 nm) and JSR Micro M35G (1.2 um). It's important to develop quickly after exposure, to avoid loss of dimensions problem. The BARC is used to minimise the intensity of the light reflected from the substrate.

Before entering in the fabrication context it's useful compare the use of DUV stepper with E-beam photolithography.

An electron beam lithography system uses a focused beam of electrons to create a pattern in an electron sensitive resist and the beam is scanned across the wafer using an electromagnetic deflection system. The advantages are resolution (<20nm), the disadvantage is that it is slower compared to Stepper, the pattern having to be exposed 1 pixel at a time.

The *ASML PAS Stepper* uses DUV photons (248nm) exposing DUV-sensitive photoresists through a mask, generally referred as the "Reticle" (explained before). The resolution in

this case should reach ~150nm. During the exposure one shot through the Reticle will expose only one small part of the wafer, called “field”. For this reason it is possible to pattern the complete wafer exposing the wafer in several shots at different positions and with different structures.

For the first fabrication, the same structure (*TS-Channels*) is used for the different dies, where dose and defocus change. Figure 5.5 shows how the wafer is divided in 3 vertical lines and 7 horizontal lines, and how the dose and defocus are swept.

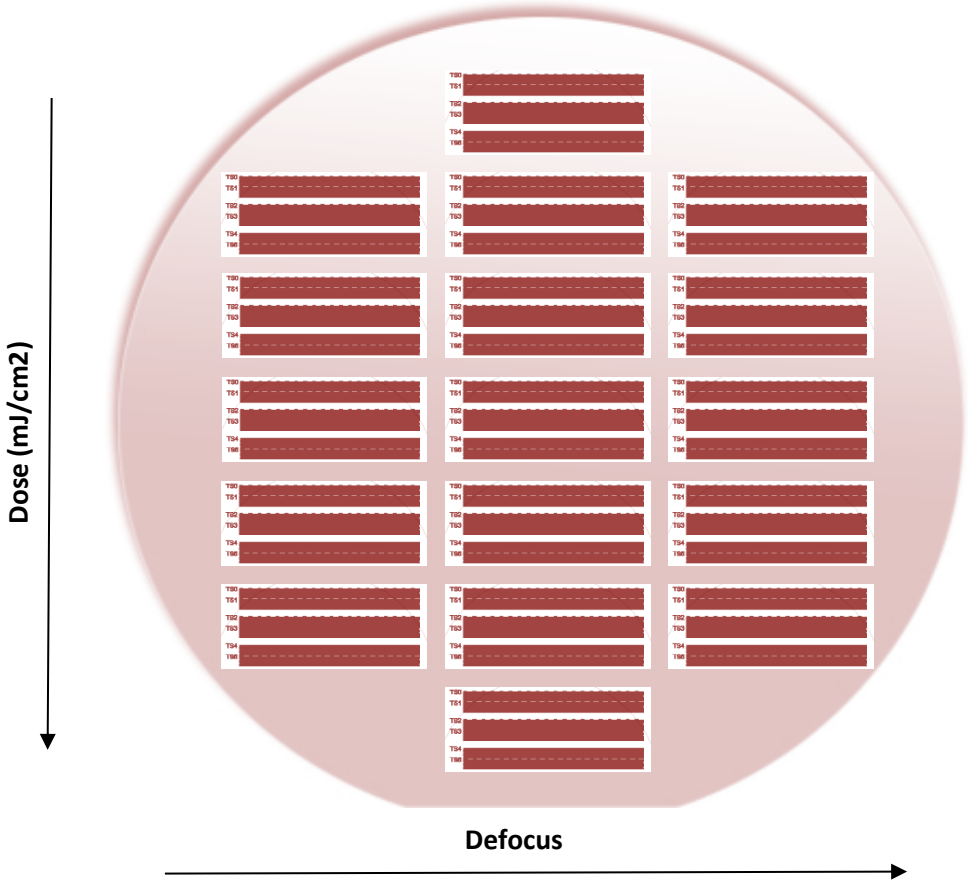

Figure 5.5: Disposition of TS- Channels in the wafer: 3 vertical lines and 7 horizontal lines

In the first fabrication, the purpose is to figure out the correct values of Dose and Defocus. In one wafer the dose is stepped for each die of the grid from the top to the bottom and with a nominal dose 31 *mJ/cm2* and a step dose 2 *mJ/cm2*. The Defocus changes from left to right with a nominal value 0 and step focus 0.3. The result is the top part being strongly

underexposed and the bottom overexposed and there aren't evident differences changing the focus. In the Figure 5.12 it will be more clear.

5.3.2: Etching of BARC and silicon nitride

The channel is etched in two steps: first the slits have to be defined in the BARC and Is-SiNx layers and then the silicon is etched through these slits. After each step it is important, for informational purpose, to know which is the photoresist thickness with *Filmetric F54* (Automated Film Thickness Mapping), to protect the surface where we don't want to etch. The Figure 5.15 will explain how the thickness changes.

Two different types of procedures to etch the BARC and Is-SiNx are compared.

In the first one the equipment used is the *SPTS Dielectric etcher*. The recipe "*BARC_Slow*", with an etch rate of 80 nm/min, is applied for 55'' to remove the BARC. The etch rate of the photoresist is 100 nm/min.

The recipe "*Si_3N_4_smooth*" is used to etch Is-SiNx for 2'30'', with an etch rate of 160 to 220 nm/min for the Si3N4 and 70 nm/min for the photoresist.

The second equipment tested is *TEL Unity Me system*, an automatic plasma etching production tool from Tokyo Electronic. The recipe "*CMI.BARC.CF4*" is used for 35'' to remove the BARC, with an etch rate of 110 nm/min for BARC and photoresist. The recipe "*CMI.SIN.OX*" is applied for 1'30'' to etch SiNx, with an etch rate of 130nm/min for SiNx and 105nm/min for the photoresist.

The parameters for the two procedures are reported in Table 5.2.

	SPTS	TEL
DUV BARC Etching	"BARC_Slow" CHF3/O2 55'' BARC etch rate = 80nm/min PR etch rate=100 nm/min	"*CMI.BARC.CF4*" *CF4* 35'' BARC etch rate=110nm/min PR etch rate=110 nm/min
SiNx Etching	"*Si_3N_4_smooth" CHF3/SF6* *2'30''* SiNx etch rate=160-220nm/min PR etch rate= 70nm/min	"*CMI.SIN.OX" CH2F2/O2/Ar* *1'30''* SiNx etch rate=130nm/min PR etch rate= 105nm/min

Table 5.2: Parameters for SPTS and TEL during the BARC and SiNx etching

This step helps not only to choose the correct dry etching procedure but also the best photoresist thickness to use. In Figure 5.6 the cross-section of the wafer with thick photoresist is represented, after TEL etching: the apertures size is 600nm in the photoresist, in the BARC it turns out halved and the Is-SiNx is not completely etched.

For the other aperture sizes the results are worse, because of their smaller sizes. There are 2 explanations for this behaviour: the high aspect ratio with the thick photoresist (1.1um for openings 600nm), and the fact that the exposure has not been optimized with the stepper.

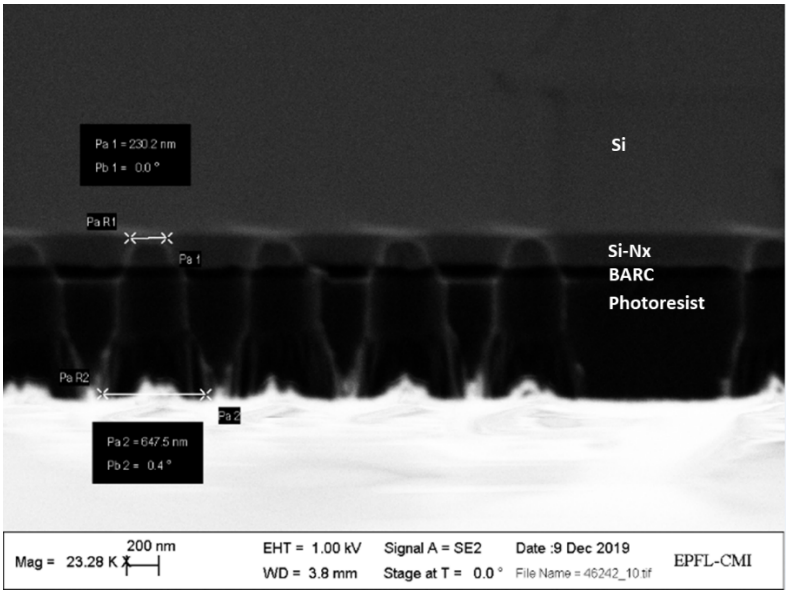

Figure 5.6: Cross Section of the wafer with thick photoresist after TEL: the aperture size is 600 nm, it turns out halved in the BARC and the SiNx is under etched

With these premises, we understand that it will be difficult to properly etch the silicon in order to realize the channel in wafer with the thick photoresist.

We don't want to optimize for long and also overetch too long. The following step is to compare the results after TEL and after SPTS on the thin photoresist.

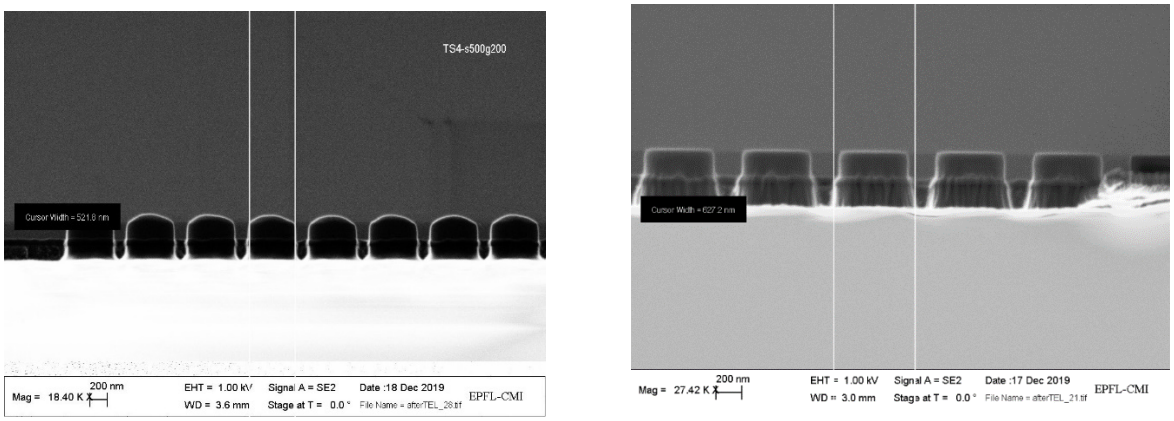

(a) (b)

Figure 5.7: Dry Etching with SPTS: the aperture size is 600nm long (a); Dry Etching with TEL: the aperture size is 600nm long (b).

In the Figure 5.7 it is possible to find out two considerations. The first one is the difference of the use of TEL with the same recipe for the wafer with the thick photoresist (Figure 5.6) and the thin one (Figure 5.7 b): the apertures have the same dimensions but in the second case the SiNx is well etched with the hole size equal to that of the photoresist.

The second one is that for the bigger holes size the results after dry etching are the same regardless of the equipment used but it is not true for the smaller holes (300 nm).

Good evidence of this is in the Figure 5.8, where the results after TEL are better compared to the results after SPTS, where the SiNx is not etched.

The membrane with the smaller size holes and the bigger gap value is the one that is of interest: with this design, we will need to deposit a thinner layer of SiNx to close the apertures, and the membrane will be more robust.

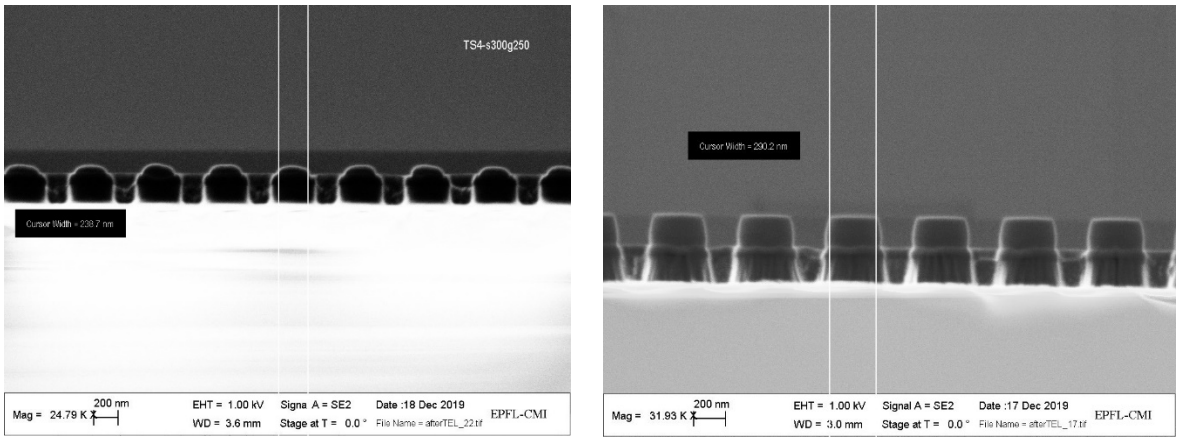

(a) (b)

Figure 5.8: Dry etching with SPTS: the aperture size is 300nm (a); Dry etching with TEL: the aperture size is 300 nm (b).

This study helps to optimize the dry etching process by using the TEL which ensures to gain positive results for each design of the channel 's membrane, with different size holes.

After the dry etching, it is of fundamental importance to inspect not only the cross section but also from the top side with SEM to figure out the best value of two parameters: the holes' correction, the dose value.

In Figure 5.9 it is clear that TS0 composed by apertures without correction have rounded corners compered to TS4 (aperture's corner has three squares with 0.4 side length) that allows to have apertures well defined, like squares.

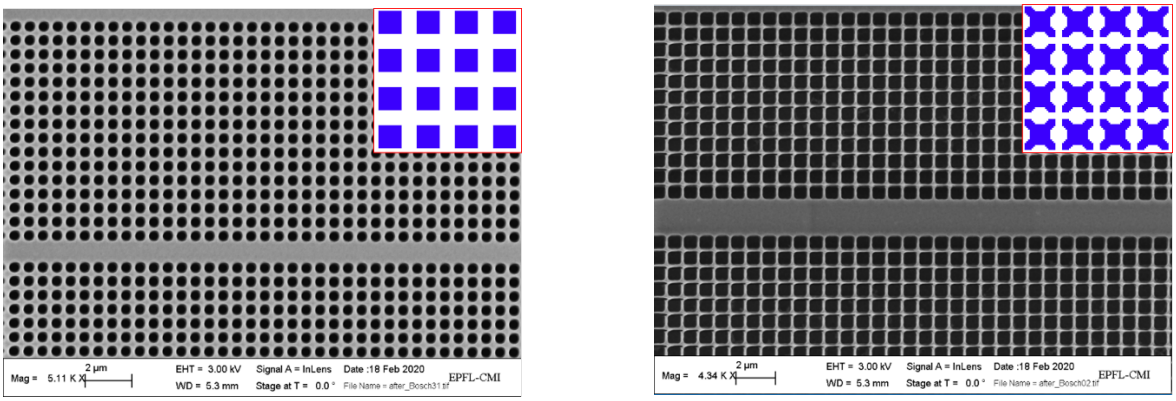

(b) (b)

Figure 5.9: TS0 without corrections: apertures 400 nm long (a); TS4 with corrections: apertures 400nm long (b).

In the Figure 5.10 the same structure, with apertures 400nm long, are represented for two different dose values: in the first one with a dose of 31 mJ/cm2 the aperture size, measured during a SEM inspection, is about 420 nm and in the second picture with a dose value of 35 mJ/cm2 the aperture size is about 480 nm, and it is overexposed.

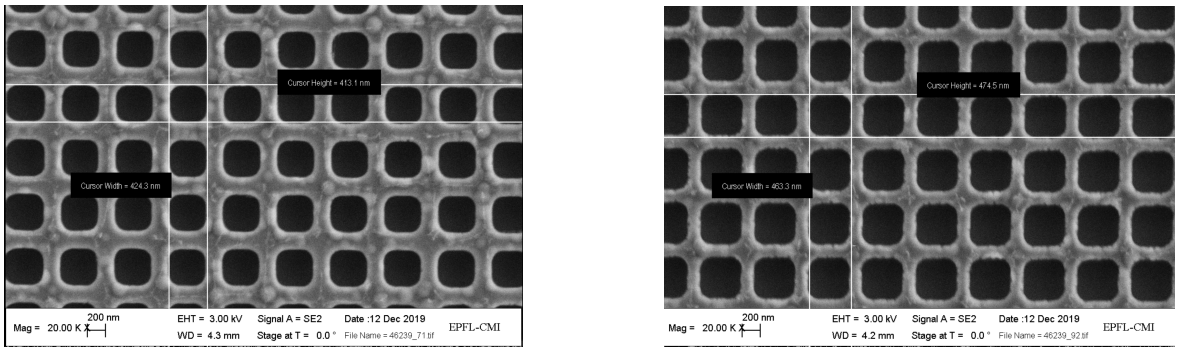

(a) (b)

Figure 5.10: TS4 with a dose value of 31mJ/cm2 (a); TS4 with a dose value of 35mj/cm2 (b).

The dose value, chosen for the following fabrications, is the nominal value 31 mJ/cm2, for all dies in the same wafer. This value enables to have the most faithful possible aperture dimensions to those of design.

These choices (photoresist, dose, test structure) allow to optimize the subsequent steps by working on each chip containing a single die, after making a single photolithography for a wafer, reducing time and costs.

Every chip to be process in the following step is manually cleaved and attached to a dummy wafer with quick stick.

5.3.3 Dry etching of Si and Wet Etching in KOH

The following step is the Bosch Process to etch the silicon through the membrane, as explained in the Paragraph 4, this process consists in alternating SF6 pulses (300 sccm) and C4F8 pulses (200 sccm) and the temperature is set to 30°C.

Figure 5.11 shows how the use of squares and non-circular openings helps to optimize the silicon etching process: reducing passivation residues under the membrane. To explain this, we compare a membrane composed of circular openings with radius equal to "*r*" with a membrane composed of squares with the side "*2r*" long. The red line around the holes represents how the gas is distributed to etch the silicon.

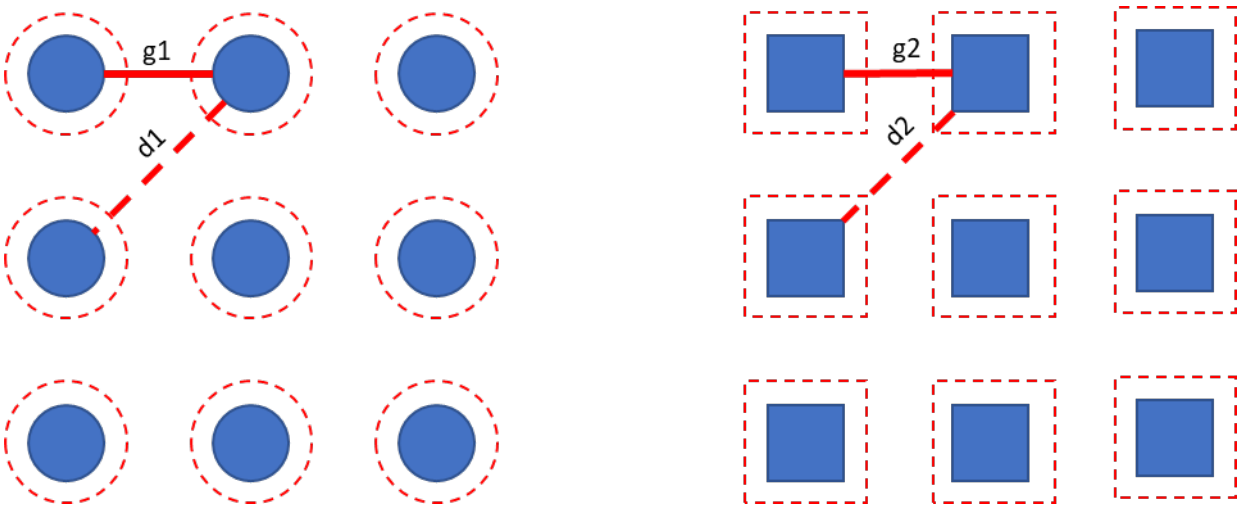

Figure 5.11: Membrane composed of circular openings (a); Membrane composed of squares openings (b).

The horizontal gap between two openings is the same for both representations, since the centre of the openings is the same:

$$g1 = g2,$$

where $g1$ is the gap between the two circles and $g2$ between the two squares.

If we calculate the diagonal gap between two openings, we will find that the value for the circles will be greater.

$$d1 = \left[(g1 + 2r)\sqrt{2}\right] - 2r$$

$$d2 = \left[(g1 + 2r)\sqrt{2}\right] - 2\frac{\sqrt{2}}{2}r,$$

where $d1$ is the diagonal distance between two circle apertures and $d2$ is the diagonal distance between two squares.

For the first type of membrane it becomes more difficult to remove Si in the channel in a diagonal direction because of a greater space, this is the reason why to use square holes, and thus the design correction TS4.

The first recipe tested for the Bosch process is "*SOI_accurate++"* for 2'06'' composed by 14 cycles, altering 7''SF6 with 2''C4F8.

This first result is good: all the channels are realized in the Si substrate also with a membrane composed of the smaller aperture size (300nm) and the bigger gap (250 nm).

Figure 5.12 shows the cross section of the channel, with a membrane composed by apertures size 400nm long and a gap 250 nm long. It is visible that the membrane are composed by SiNx, BARC and Photoresist, with the apertures through which the Si is etched. The number of corrugations is the same as the cycles number, in this case 14. If the SF6 pulse is shorter, while maintaining the total SF6 time, the number of corrugations is higher with a small scalloping width on the edges of the channel. This could be a good option to have a smoother channel wall but a disadvantage of this time multiplexed process is to get more passivation.

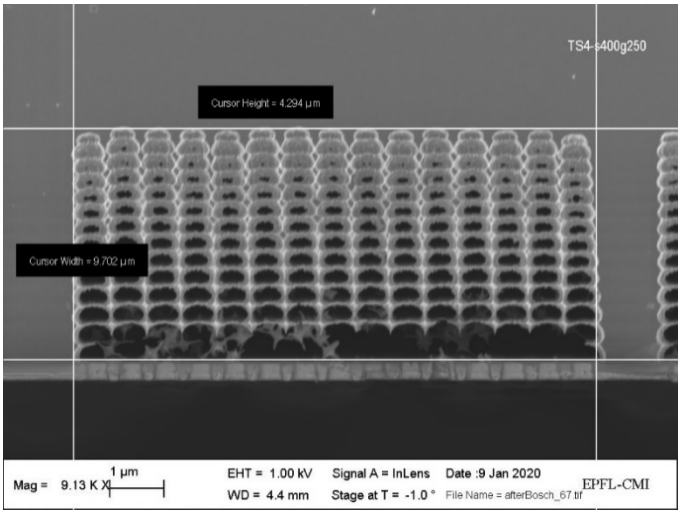

Figure 5.12: After Bosch for 2'06'' with 14 cycle of 7'' SF6 and 2''C4F8. There are passivation residues inside the cavities. The 14 pulse of SF6 are responsible for the visible scalloping on the walls.

Before stripping the photoresist after the Bosch process it is useful to report how the photoresist thickness value decreases after each step (Figure 5.13). Knowing the etching rates of the different processes will help keeping the integrity of the membrane, avoiding that we consume all the photoresist and start etching the silicon nitride.

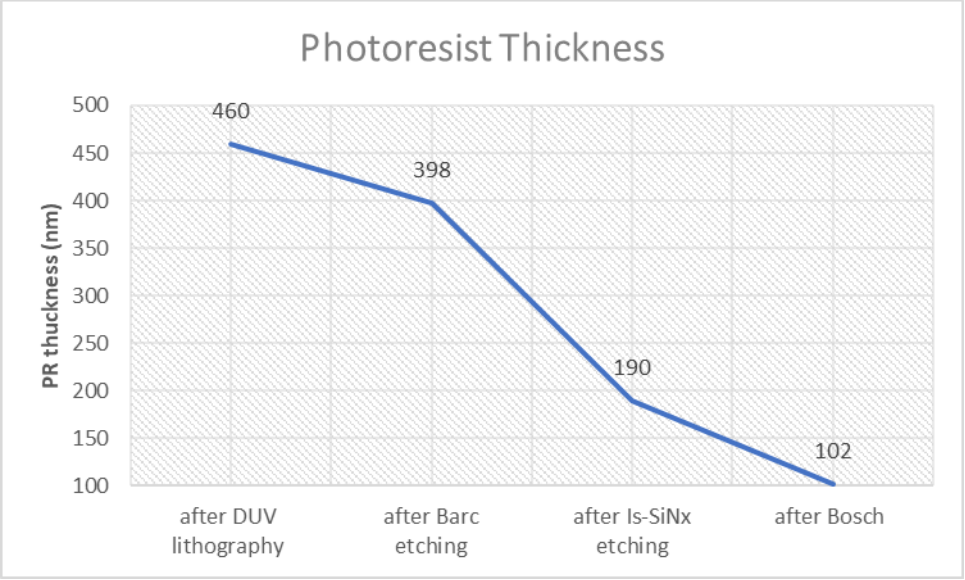

Figure 5.13: How the thickness of the photoresist changes after each steps.

The photoresist is then stripped at full-wafer level in different steps. At first we use "*Tepla Plasma Stripper"* [22] with high Power Plasma for 1' following by a *Wet etching* with Remover 1165 to remove the photoresist and at the end *Tepla* with high Power Plasma for 3' to remove the BARC. The Wet etching is composed by three steps: two baths in Remover 1165 each for 5' at 70°C, and a bath in Cascade H2O 5' for three times.

With a chip this procedure is different: as explained before, the wafer is cleaved to allow to compare different etching procedures on different chips with the same test structure. To remove the quick stick, after detaching it from the dummy wafer, the chip is immersed in acetone and subsequently in IPA. In Figure 5.14 it is showed as after this step the membrane is dirty and it is possible to see residues on the channel.

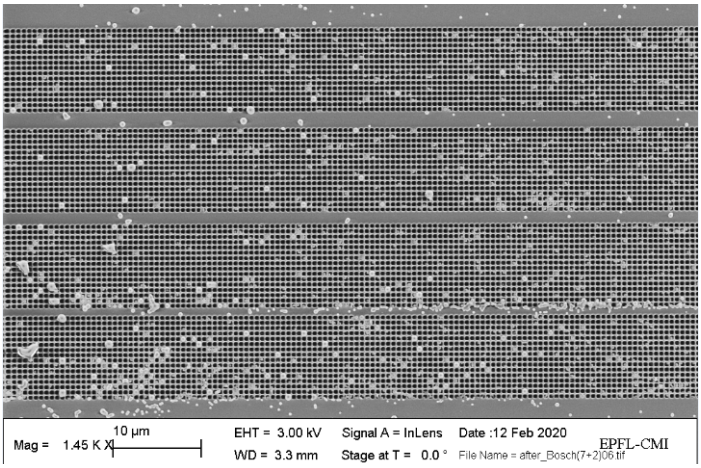

Figure 5.14: SEM picture of the membrane from the Top side.

The residues are not only from the quick stick but in particular for the passivation process. For this reason a wet KOH etching has been used to clean inside the channel and to achieve the least scalloped profile possible.

Different KOH steps are tested: increasing the etching time from 1’ to 7’ at Room Temperature or for 20’’ at high temperature 70°C. The Figure 5.15 attested that even after the use of high temperature it is not possible to clean the channel.

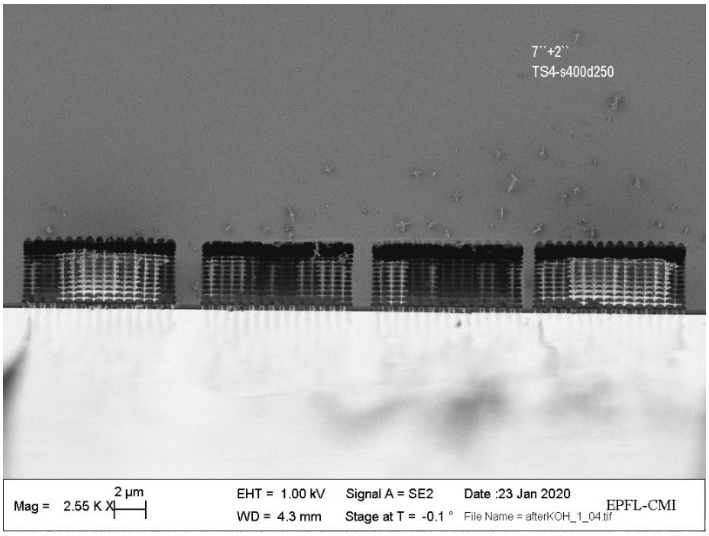

Figure 5.15: SEM picture of the cross section of the channels after “SOI_accurate++” and KOH at 70°C for 20’’.

To prevent this problem, it is necessary to increase the etching time in the Bosch process, from 7’’ to 8’’ to reduce passivation residues, using the recipe “*SOI_accurate ++++*”.

In the Figure 5.16 we report the result after the use this new Bosch process for 10 cycles.

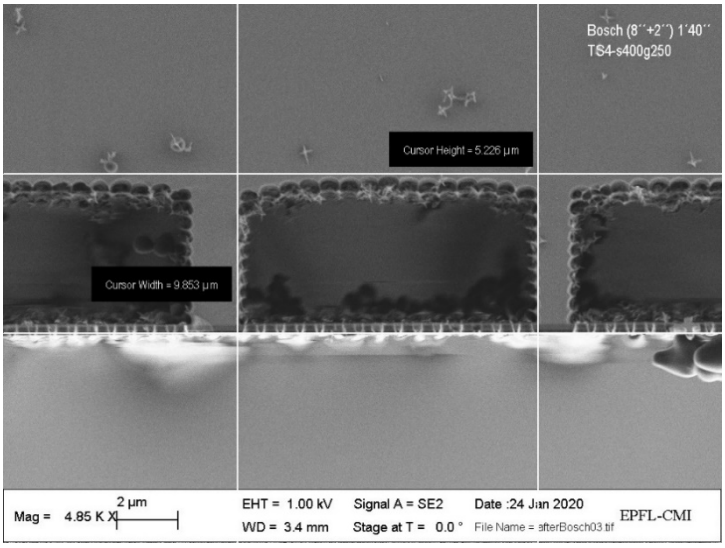

Figure 5.16: SEM picture of the cross section of the channels after Bosch process “SOI_accurate++++”.

In comparison to Figure 5.12, it is clear that despite having a membrane with the same dimensions, with 10 cycles of this new Bosch process (8" SF6 + 2" C4F8) the passivation residues are presented only in the channels edges.

Comparing the features of the channel after these two different Bosch processes helps to study the influence of the applied time and the chosen recipe. It is possible to inspect how the length and width of the channels change, even the wall thickness, especially the minimum distance (1 um), to be sure that there isn't connection between the two closest channels.

The first graph, in Figure 5.17, analyses the channel width for the different Test Structure. The ideal value used for the design is compared with the values obtained after Bosch (7" + 2") and Bosch (8" + 2"). It is clear that both don't diverge by more the 5% from the design values, but an increase in the attack time (SF6) leads to an increase in channel width.

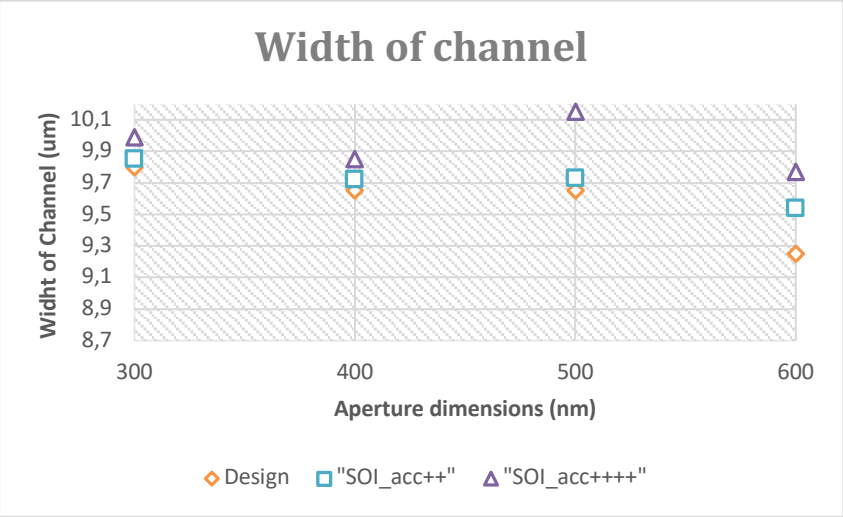

Figure 5.17: Graph of the channel widths in the design, after Bosch (7"+2") or after Bosch (8"+2").

It is possible to measure the depth of the channel only through the cross section. The graph, in Figure 5.18, confirms that if we compare the depth of the channels with openings of different sizes, following the same Bosch process, it will be greater if the openings are larger. A further consideration is that with an increase in the etching time there is a trend increase in depth.

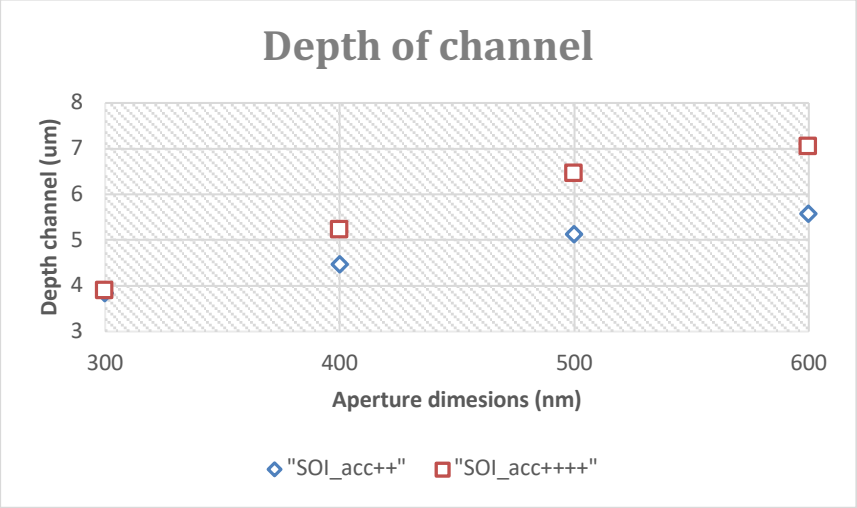

Figure 5.18: Graph of the channel depths in the design, after Bosch (7"+2") or after Bosch (8"+2").

The last characteristic to specify is the width of the wall. As explained above, it is important to understand what is the minimum achievable distance between two channels. The graph in Figure 5.19 shows the evolution of the minimum dimension used in the design, 1um. After entering both processes this value will be reduced: in the first case by a maximum of 51% and in the second one of 67%.

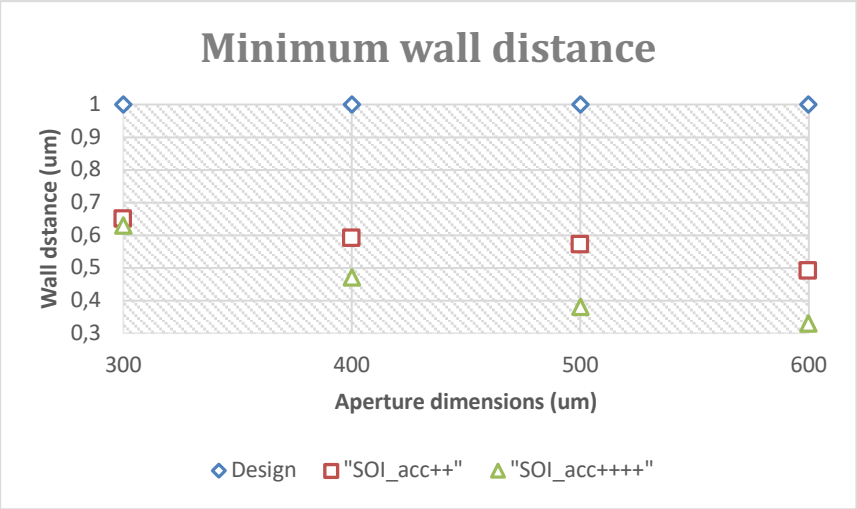

Figure 5.19: Graph of the minimum wall distance in the design, after Bosch (7"+2") or after Bosch (8"+2").

At the end it's clear that to increase etching times leads to increase the depth of the channel and the etching/passivation ratio.

Choosing the Bosch process with a longer etching time, we then immerse the wafer in KOH for 3' at Room temperature, following by a neutralization in HCl for 2h, to complete the wet etching.

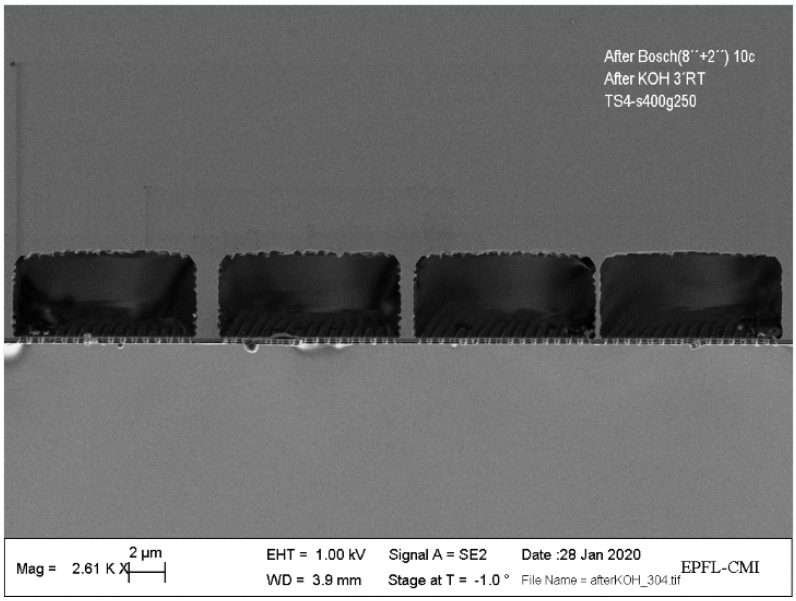

Figure 5.20: SEM picture of the channel cross section after Bosch process (8"+2") and KOH at RM for 3' .

The result is good, the channel is clean inside and the surface is well smoothed (Figure 5.20).

In the Figure 5.21, it is reported how the channel features (width, depth, wall distances) change after the etching process (dry etching, wet etching) compared to the design values. We analyze the channel with the smaller aperture dimensions (300 nm) and bigger gap (250 nm).

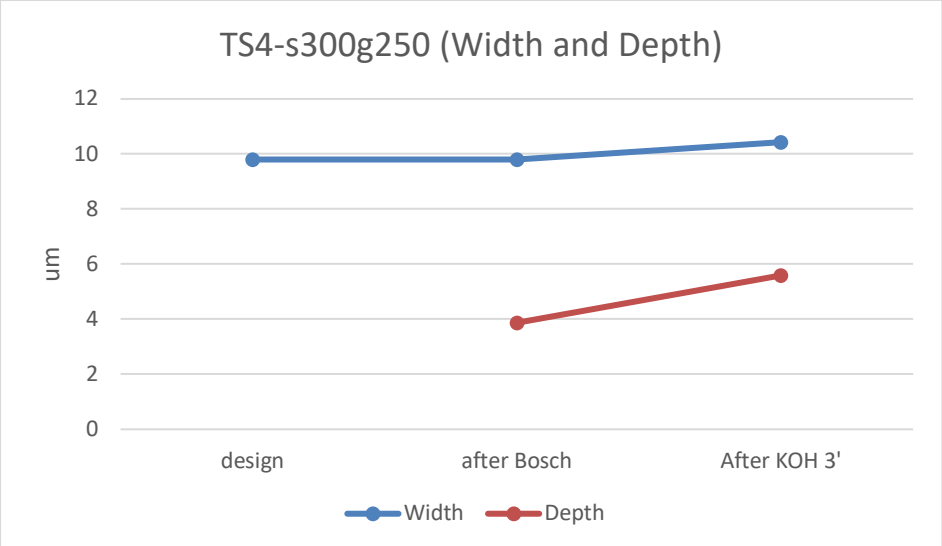

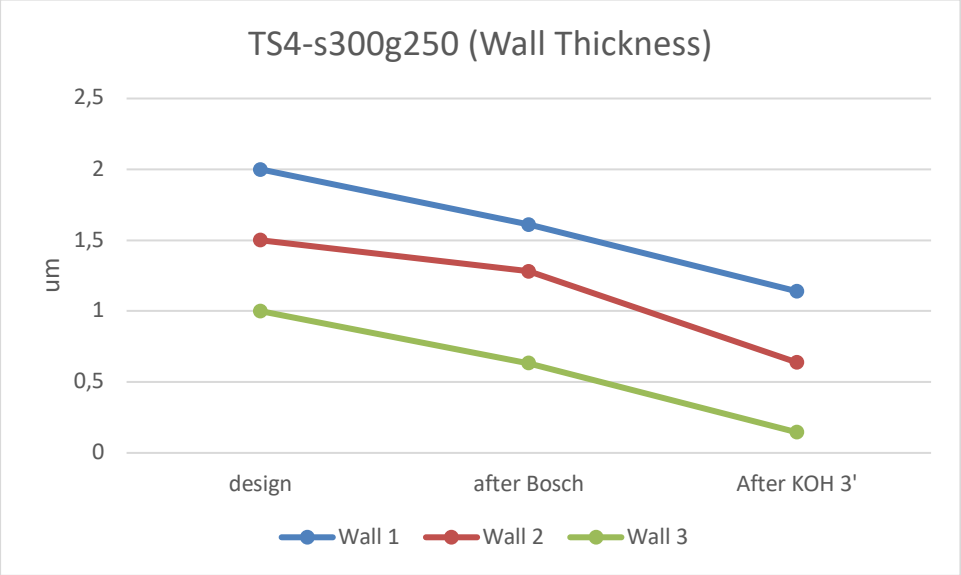

Figure 5.21 Graph of all channels features with aperture 300nm long and the gap 250nm long, calculated after each steps.

5.3.4 Sealing with nitride Low Pressure Chemical Vapor Deposition (LPCVD)

Once all the steps are optimized, the process is repeated in a full wafer (Appendix B - Fabrication 4). At the end, the wafers are cleaned with RCA process formed by CMi staff, to remove the organic and metallic residues through several baths.

A 250 nm layer of low-stress silicon nitride is deposited on the membrane in order to fill up the apertures and to cover the silicon channel walls below the membrane. The deposition is done by the reaction between dichlorosilane (SiH2Cl2) and ammonia (NH3) at 820°C to 850°C, with a pressure of 200mTorr.

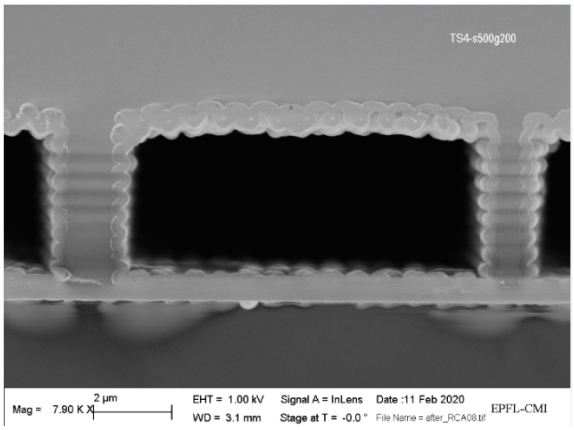

Figure 5.22: SEM picture of the channel cross section after the deposition of 250 nm of Is-SiNx. The membrane has apertures 600 nm long.

The results after the deposition are completely different from the results obtained with the chip: only the channels with the largest aperture membrane size, 500nm and 600nm with the smallest gap, 200nm are opened, such as in Figure 5.22.

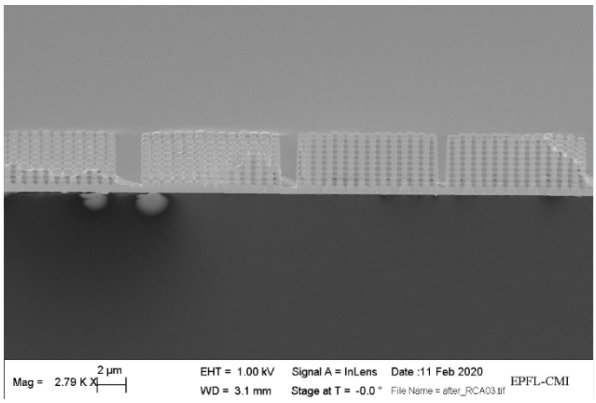

Figure 5.23: SEM picture of the channel cross section after the deposition of 250 nm of Is-SiNx. The membrane has apertures 400 nm long.

In the Figure 5.23 it is evident that the channel, with openings of 400 nm in length, was not cleaned inside before the deposition. There were passivation residues filled in turn by Is-SiNx deposited at the end.

The reason could be related to the Bosch process: processing at chip level, the use of Quick Stick may have lead to a lower thermal conductivity between the chip and the chuck of the etching machine. The consequence would be a more important chemical etching due to the higher temperature.

Using this process on the full wafer might require a different duration or different recipes to achieve good results. A further motivation could be the use of the wet bench to remove the photoresist, as some photoresist residues could pass through the membrane and settle in the channel.

5.4 Comments and Conclusions

The fabrication of the channels is based on the etching of Silicon covered by a structural layer of low-stress silicon nitride (Is-SiNx) of 200nm.

DUV lithography allows to reproduce the squares in the DUV photoresist (JSR M108Y (470 nm) which will define the channel membrane in Is-SiNx with a dry etching (TEL).

The microchannel walls are defined by the Bosch process and cleaned with KOH and filled with LPCVD Is-SiNx.

Several parameters were optimized during the different phases. The correct exposure dose is obtained by studying the dimensions of the squares.

The fabrication of "*TS-Channel*" studies how to create a channel with a membrane composed of apertures. We target small openings and a greater gap in order to reduce the deposition time of silicon nitride and maintain a good robustness of the membrane.

The dry etching in the BARC and Is-SiNx must guarantee the passage of gas during the Bosch process to create the cavity in Si. The Bosch process and the KOH etching are chosen in order to make a cleaned and smoothed channel.

The process optimized during the chip fabrication does not give the same positive results in the full wafer fabrication: the etching steps need different parameters and it is important to check how clean the membrane is after each step to avoid that some residues might travel inside the channel.

Once optimized the membrane parameters with the test structure, cantilever shaped channels will be made with same characteristics.

6 Conclusions and outlooks

The goal of this project focuses on the optimization of SMR developed in the prior art. This device is a micro-channel resonator with embedded PZE electrodes in order to provide electrical actuation and readout. The main issue of this fabrication is the presence of parasitic capacitance. To circumvent this problem, we worked on two distinct aspects of the fabrication: electrode and channel.

PZE electrodes were fabricated reducing the surface of electric tracks and the overlapping area between top and bottom contacts. The fabrications gave us positive results for the conductivity of the metal and the insultation between top and bottom of different chips.

We will continue to characterize all the chips fabricated, in order to compare the results with the prior analyses.

For the channels we etched in Si instead of polysilicon doped, and the conducting layer is not present anymore. The Design was realized in order to optimize channel membrane features: aperture sizes, gap values and the wall thickness. We used the DUV lithography instead of EBEAM lithography reducing the process time but losing in resolution.

We optimized all channel parameters working on single chip. The idea for the following fabrication is to restart the fabrication working on a full wafer, since the etching features could be different. After each step it will be fundamental to check the top of the wafer and the cross section with SEM, to ensure the cleaning of the membrane and the etching of the Si through it. After tests done on this structure to determinate designs for the membrane and the sidewalls of channels, we will fabricate hollow beams.

Once those two fabrications are completed, we will work on an single fabrication of a microchannel with embedded PZE electrodes, and move towards experiments.

References

[1] Elise A. Corbin, Fang Kong, Chwee Teck Lim, William P. King and Rashid Bashir "Biophysical properties of human breast cancer cells measured using silicon MEMS resonators and atomic force microscopy"

[2] Marija Plodinec, MarkoLoparic, Christophe A.Monnier, EllenC.Obermann, Rosanna Zanetti-Dallenbach, Philipp Oertle, JanneT.Hyotyla, Ueli Aebi, Mohamed Bentires-Alj, Roderick Y. H. Lim and Cora-Ann Schoenenberger "The nanomechanical signature of breast cancer"

[3] Małgorzata Lekka, Dorota Gil, Katarzyna Pogoda, Joanna Dulińska-Litewka, Robert Jach, Justyna Gostek, Olesya Klymenko, Szymon Prauzner-Bechcicki, Zbigniew Stachura, Joanna Wiltowska-Zuber, Krzysztof Okoń, Piotr Laidler "Cancer cell detection in tissue sections using AFM"

[4] Pei-Hsun Wu, Dikla Raz-Ben Aroush, Atef Asnacios, Wei-Chiang Chen, Maxim E. Dokukin, Bryant L. Doss, Pauline Durand-Smet, Andrew Ekpenyong, Jochen Guck, Nataliia V. Guz, Paul A. Janmey, Jerry S. H. Lee, Nicole M. Moore, Albrecht Ott, Yeh-Chuin Poh, Robert Ros, Mathias Sander, Igor Sokolov, Jack R. Staunton, Ning Wang, Graeme Whyte & Denis Wirtz "A comparison of methods to assess cell mechanical properties"

[5] D. Ramos, J. Tamajo, J. Mertens and M.Calleja "Origin of the response of nanomechanical resonators to bacteria adsorption"

[6] Javier Tamayo, Priscila M. Kosaka, José J. Ruz, Álvaro San Paulo and Montserrat Calleja "Biosensors based on nanomechanical systems"

[7] Silvan Schmid, Luis Guillermo Villanueva, Michael Lee Roukes "Fundamentals of Nanomechanical Resonators"

[8] A.De Pastina, "PZE-transduced Suspended Microchannel Resonators for sensing applications"

[9] Thomas P. Burg, Michel Godin, Scott M. Knudsen, Wenjiang Shen, Greg Carlson, John S. Foster, Ken Babcock & Scott R. Manalis "Weighing of biomolecules, single cells and single nanoparticles in fluid"

[10] M. Gurtin, X. Marchenscoff and R. Thurston, "Effect of surface stress on the natural frequency of thin frequency of thin cristal"

[11] Anja Boisen, Søren Dohn, Stephan Sylvest Keller, Silvan Schmid and Maria Tenje "Cantilever-like micromechanical sensors"

[12] T. P. Burga and S. R. Manalisb "Suspended microchannel resonators for biomolecular detection"

[13] S. Schmid, B. Malm, A. Boisen “Quality factor improvement of silicon nitride micro string resonators”

[14] D Ramos, J Tamayo, J Mertens, M Calleja, L G Villanueva and A Zaballos “Detection of bacteria based on the thermomechanical noise of a nanomechanical resonator”

[15] A. De Pastina, D. Maillard, L.G. Villanueva “Fabrication of suspended microchannel resonators with integrated piezoelectric transduction”

[16] https://cmi.epfl.ch/photo/EVG150.php

[17] https://cmi.epfl.ch/photo/MLA150.php

[18] https://cmi.epfl.ch/thinfilms/Spider600.php

[19] Cleland A N, Pophristic M and Ferguson I 2001 Single-crystal aluminum nitride nanomechanical resonators Appl. Phys. Lett. 79 2070

[20] https://cmi.epfl.ch/photo/ACS200Gen3.php

[21] https://cmi.epfl.ch/etch/STS.php

[22] https://cmi.epfl.ch/etch/Tepla.php

[23] https://cmi.epfl.ch/etch/APS.php

[24] https://cmi.epfl.ch/etch/AMS200.php

[25] Banqiu Wu, Ajay Kumar, and Sharma Pamarthy “High aspect ratio silicon etch”

[26] Zoé Daguin, L. G. Villanueva, A. De Pastina, D. Maillard “Fabrication of suspended microchannel resonators for biosensing application

Appendix A

Process Flow – Electrodes

Technologies used
Photolithography, Sputtering, Lift-off, Dry etching, Wet etching, PR strip

Ebeam litho data - Photolitho masks - Laser direct write data			
Mask #	*Critical Dimension*	*Critical Alignment*	*Remarks*
1	**2um**	First Mask	Bottom electrode
2	**2um**	2um	Top electrode
3	**2um**	2um	Release

Substrate Type
Silicon <100>, Ø100mm, 525um thick, Single Side polished Layer: 500nm low-stress silicon nitride

Step	Process description	Cross-section after process
0	State of the wafer at the beginning of the process	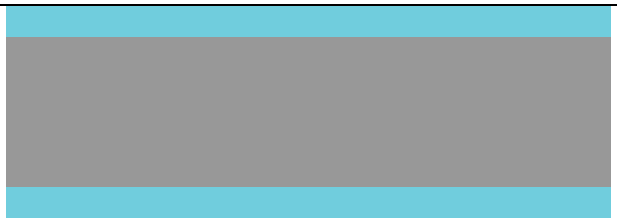
1	Photolitography: coating Material: AZ1512 on LOR 5A Machine: Z6 – EVG150 Thickness: 0.4µm LOR, 1.1µm, AZ1512	

2	Photolithography: Exposure Machine: Z16 – MLA150 Exposure dose: 60mJ/cm2	
3	Photolithography: Development Machine: Z6 – EVG150	
(4)	O2 plasma Z2: Tepla 10” Strip low	
4	Sputter deposition Materials: AlN + Pt Machine: Z4 – SPIDER600 Target: 15nm + 25nm	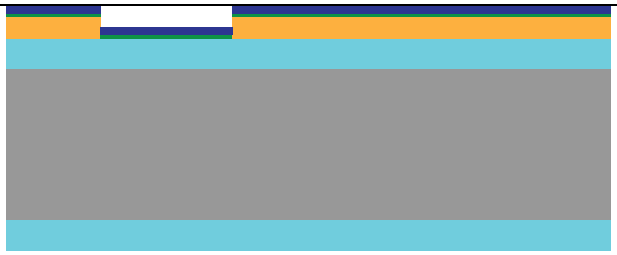
5	Lift-off Materials : PR + AlN + Pt Machine: Z1 – Photolitho bench	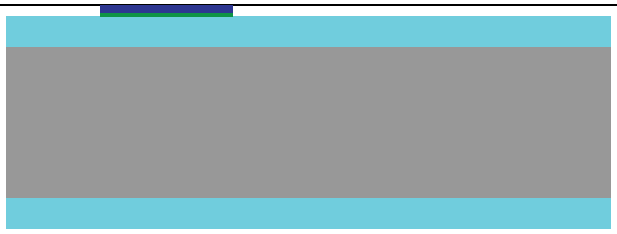
6	Inspection Machines: Z1 – Microscope, Z1 – Zeiss LEO	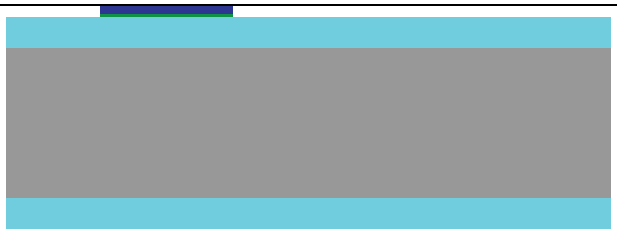

7	Sputter deposition Materials: AlN + Pt + SiO2 Machine: Z4 – SPIDER600 Target: 300nm + 25nm + 20nm	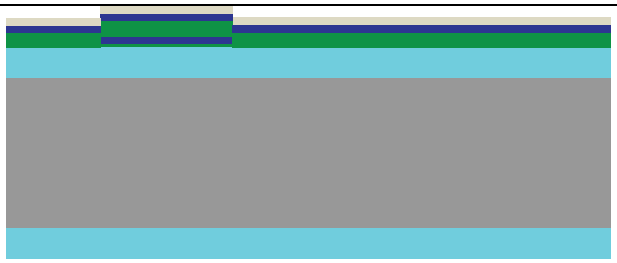
8	Photolitography: coating Material: AZ ECI 3027 Machine: Z1 – RiteTrack Thickness: 2µm	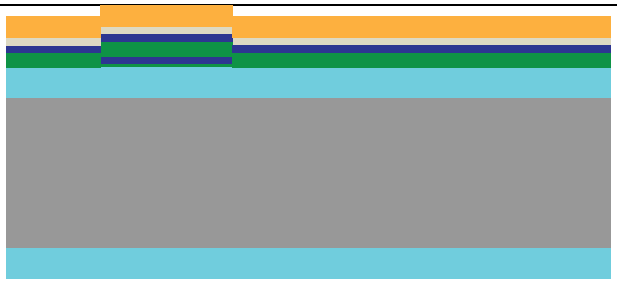
9	Photolithography: Exposure Machine: Z16 – MLA150 Exposure dose:	
10	Photolithography: Development Machine: Z1 – RiteTrack	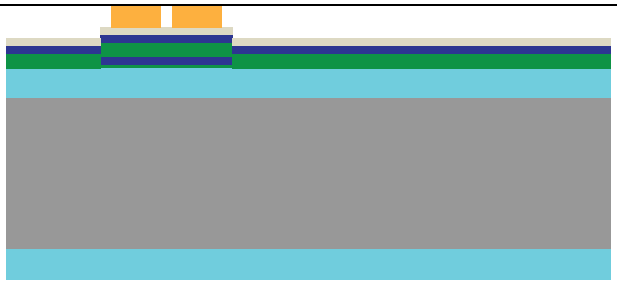
11	Anisotropic dry etch Materials : SiO2/Pt/AlN Machine: Z2 – STS Depth : 20nm + 25nm + 300nm	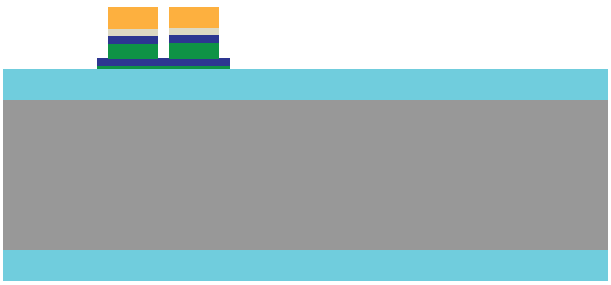
12	Photoresist strip Materials : AZ ECI Machine: Tepla Z2 1min process high + remover 1165 UFT wet bench).	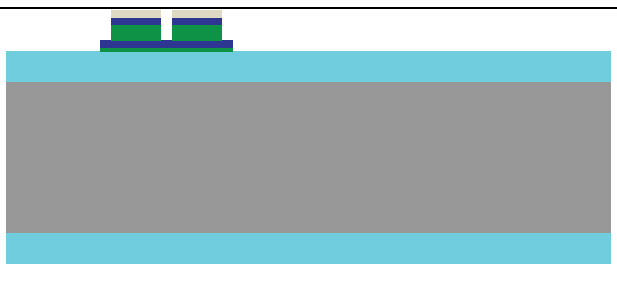

13	Wet etching Materials : SiO2 Machine: Z14 – Arias Acid Bench	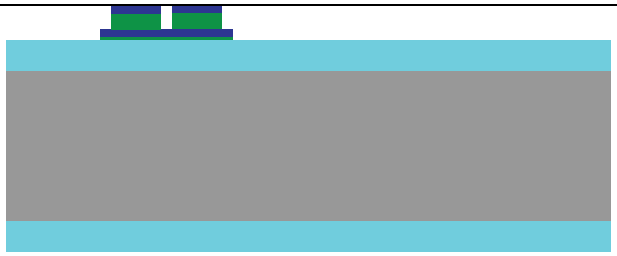
14	Inspection Machines: Z1 – Microscope, Z1 – Zeiss LEO	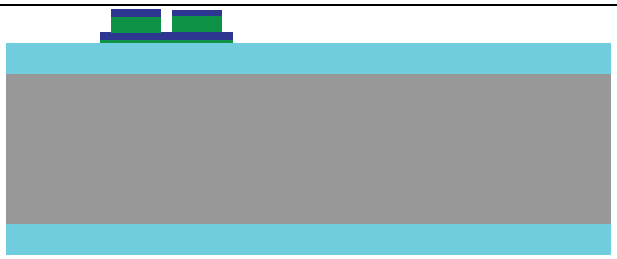
15	Photolitography: coating Material: AZ ECI 3027 Machine: Z1 – RiteTrack Thickness: 5µm	
16	Photolithography: Exposure Machine: Z16 – MLA150 Exposure dose:	
17	Photolithography: Development Machine: Z1 – RiteTrack	
18	Anisotropic dry etching Materials : ls-SiNx/Si Machine: Z2 – AMS200 Depth : 500nm + 20µm	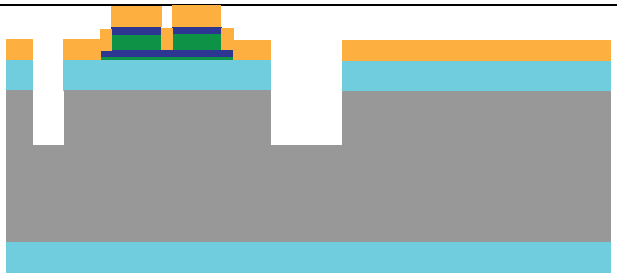

19	Isotropic dry etching Materials : Si Machine: Z2 – AMS200 Lateral depth : 20µm	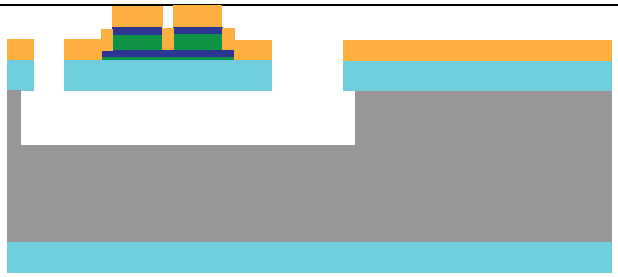
20	PR strip: O2 plasma Z2: Tepla 1’ Strip high	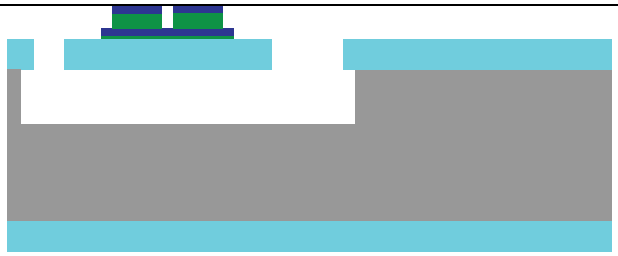
21	Photoresist strip Materials : AZ ECI Machine: Z2 – UFT	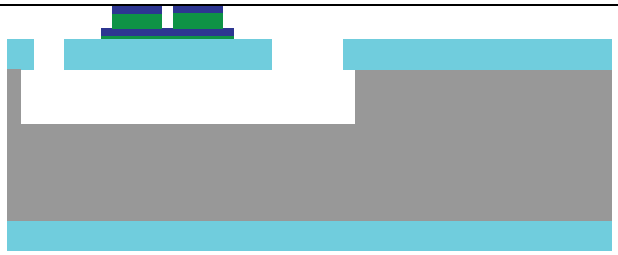
22	Inspection Machines: Z1 – Microscope, Z1 – Zeiss LEO	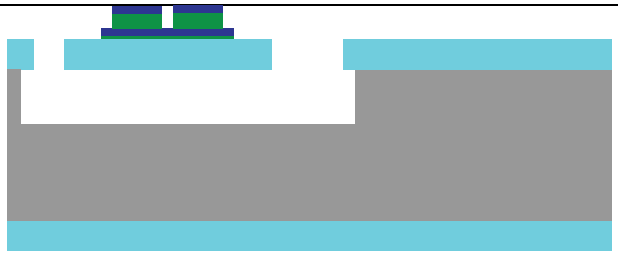

Fabrication 1

Process	Equipment	#38970	#38983	#38972
Coating Bottom Contact	**Z6- EVG150**	Material: AZ1512 +LOR 5A Thickness: 0.4 um LOR 1.1um AZ1512	Material: AZ1512 +LOR 5A Thickness: 0.4 um LOR 1.1um AZ1512	Material: AZ1512 +LOR 5A Thickness: 0.4 um LOR 1.1um AZ1512
Exposure Bottom Contact	**Z16- MLA150**	Dose: 50mJ/cm^2 Non invert Defoc -1	Dose: 50mJ/cm^2 Non invert Defoc -1	Dose: 60mJ/cm^2 Non invert Defoc -1
Development Bottom Contact	**Z6- EVG150**	2X Dev_AZ1512onLOR_400nm	2X Dev_AZ1512onLOR_400nm	2X Dev_AZ1512onLOR_400nm
Inspection Bottom Contact	**Microscope**	Fences		
Sputter Deposition Bottom Contact	**Z4-SPIDER600**	Materials: AlN+Pt 20' AlN_Clean + 5'Pt_Clean 15nm AlN 18'' N2/Ar 40/10sccm SP: 1500 W Bias: 6W Temp: Room T 25 nm Pt 14'' Ar 5sccm SP: 500W Bias:/ Temp:Room T	Materials: AlN+Pt 20' AlN_Clean + 5'Pt_Clean 15nm AlN 18'' N2/Ar 40/10sccm SP: 1500 W Bias: 6W Temp: Room T 25 nm Pt 14'' Ar 5sccm SP: 500W Bias:/ Temp:Room T	Materials: AlN+Pt 20' AlN_Clean + 5'Pt_Clean 15nm AlN 18'' N2/Ar 40/10sccm SP: 1500 W Bias: 6W Temp: Room T 25 nm Pt 14'' Ar 5sccm SP: 500W Bias:/ Temp:Room T
Lift-off Bottom Contact	**Z1-Photolithography Bench**	17/10/19 15:30 h --> 21/10/19 16:16 h	17/10/19 15:30 h --> 21/10/19 16:16 h	17/10/19 15:30 h --> 21/10/19 16:16 h
Inspection Bottom Contact	**Microscope**	Lift-off not good	Fences near the edges	Fences near the edges
Sputter Deposition Active Layer	**Z4-SPIDER600**	Materials: AlN+Pt 20' AlN_Clean + 5'Pt_Clean 100nm AlN 2' N2/Ar 40/10sccm	Materials: AlN+Pt 20' AlN_Clean + 5'Pt_Clean 25nm AlN 30s N2/Ar 40/10sccm	Materials: AlN+Pt 20' AlN_Clean + 5'Pt_Clean 50nm AlN 1' N2/Ar 40/10sccm

		SP: 1500 W Bias: 6W Temp: 300° C 25 nm Pt 14s Ar 5sccm SP: 500W Bias:/ Temp:Room T RP/= 0	SP: 1500 W Bias: 6W Temp: 300° C 25 nm Pt 14s Ar 5sccm SP: 500W Bias:/ Temp:Room T	SP: 1500 W Bias: 6W Temp: 300° C 25 nm Pt 14s Ar 5sccm SP: 500W Bias:/ Temp:Room T
Coating Top Contact	**ACS200**	Material: AZ ECI 3007 + HDMS Thickness: 1.5 um	Material: AZ ECI 3007 + HDMS Thickness: 1.5 um	Material: AZ ECI 3007 + HDMS Thickness: 1.5 um
Exposure Top Contact	**Z16- MLA150**	Dose: 220mJ/cm^2 Invert Defoc -1	Dose: 200mJ/cm^2 Invert Defoc -1	Dose: 210mJ/cm^2 Invert Defoc -1
Development Top Contact	**ACS200**	V	V	V
Inspection Top Contact	**Microscope**	Resolution and alignment	Resolution and alignment	Resolution and alignment
Anisotropic dry etch Top Contact	**Z2 – STS**	AlN_etch: Launch 1':30s and check the change of curves --> 1':15''	AlN_etch: Launch 2' and check the change of the color --> 1':7''	AlN_etch: Launch 2' and check the change of the color --> 1':5''
Photoresist strip Top Contact	**Tepla Z2 or Wet Etching**	Tepla: Strip_High, 5'	Wet Etching with Remover 1165: -5' Bath Remover 1165 70° -5' Bath Remover 1165 -QDR bath rinsing cycle -Cascade bath H20 Tepla: Strip_High 30''	Wet Etching with Remover 1165: -5' Bath Remover 1165 70° -5' Bath Remover 1165 -QDR bath rinsing cycle -Cascade bath H20 Tepla: Strip_High 30''
Probing electrodes	**Probe Station**	Not good isolation from bottom and top (see the file Excel)	Good values of Resistance (R >= MΩ) (see the file Excel) Non good value for the bott to bott, it needs more etching	I°: the etching is not completed there is still Pt on the top Electrodes (see the file Excel)

Inspection	**Zeiss LEO SEM**	There are a lot of fences in the edges of the top Electrodes (see pictures)		There aren't fences in the top contact. The color of the bottom is darker because of under etching
Anisotropic dry etch Top Contact	**Z2 – STS**			Dummy 5' for the cleaning "O2_cleaning" AlN_etch 10''
Photoresist strip Top Contact	**Tepla Z2**	Strip_High 1'		
Wet Etching		KOH 40% HCl 37% (2 h)	KOH 40% HCl 37% (2 h)	KOH 40% HCl 37% (2 h)
Probing electrodes	**Probe Station**	Bad conductivity for fancing	The R between different contacts is lower	Good values of Resistance (R >= MΩ) (see the file Excel)
Coating Release	**Z01- RiteTrack Or ACS200**	RiteTrack Photoresist: AZ ECI 3027 4um	ACS200 Recipe 0147 : AZ9221 4um with HMDS, no EBR	RiteTrack HDMS 20' Photoresist: AZ ECI 3027 4um
Exposure Release	**Z16- MLA150**	Dose: 400mJ/cm^2 Invert Defoc -2	Dose: 225mJ/cm^2 Invert Defoc 2	Dose: 400mJ/cm^2 Invert Defoc -2
Development Release	**Z01- RiteTrack Or ACS200**	RiteTrack	ACS200 Recipe 0947 : AZ9221	RiteTrack
Is-SiNxEtching	**SPTS**	"Si_3N_4 smooth": 2'50''	"Si_3N_4 smooth": 2'50''	"Si_3N_4 smooth": 2'50''
Bosch Process	**AMS**	"SOI_accurate--": 2' Target: 10um **Material etch rate (µm/min): 3 to 4.5**	"SOI_accurate--": 10' Target: 40um **Material etch rate (µm/min):3 to 4.5**	"SOI_accurate--": 10' Target: 40um **Material etch rate (µm/min):3 to 4.5**
Release	**AMS**	"Si_release": 3'+2' COMPLETED! Target: 30um (15um per side) **Material etch rate (µm/min):≈2 in lateral**	"Si_release": 5' Target: 30um (15um per side) **Material etch rate (µm/min):≈2 in lateral**	 **Material etch rate (µm/min):≈2 in lateral**

Inspection	**Microscope**		20% broken cantilevers Fencing residues underneath the cantilever	
Release			"Si_release": 4':30'' in steps Target: 30um (15um per side) **Material etch rate (µm/min):≈2 in lateral**	

Fabrication 2

Process	Equipment	#85957	#85959
Coating Bottom Contact	**Z6- EVG150**	Material: AZ1512 +LOR 5A Thickness: 0.4 um LOR 1.1um AZ1512	Material: AZ1512 +LOR 5A Thickness: 0.4 um LOR 1.1um AZ1512
Exposure Bottom Contact	**Z16- MLA150**	Dose: 50mJ/cm^2 Non invert Defoc -1	Dose: 60mJ/cm^2 Non invert Defoc -1
Development Bottom Contact	**Z6- EVG150**	2X Dev_AZ1512onLOR_400nm	2X Dev_AZ1512onLOR_400nm
Inspection Bottom Contact	**Microscope**	v	v
Sputter Deposition Bottom Contact	**Z4-SPIDER600**	Materials: AlN+Pt 20' AlN_Clean + 5'Pt_Clean 15nm AlN 18'' N2/Ar 40/10sccm SP: 1500 W Bias: 6W Temp: Room T 25 nm Pt 14'' Ar 5sccm SP: 500W Bias:/ Temp:Room T	Materials: AlN+Pt 20' AlN_Clean + 5'Pt_Clean 15nm AlN 18'' N2/Ar 40/10sccm SP: 1500 W Bias: 6W Temp: Room T 25 nm Pt 14'' Ar 5sccm SP: 500W Bias:/ Temp:Room T
Lift-off Bottom Contact	**Z1-Photolithography Bench**	13-01 h 10:15 15-01 h 10:30	13-01 h 10:15 15-01 h 10:30
Inspection Bottom Contact	**Microscope**	v	v
Sputter Deposition Active Layer	**Z4-SPIDER600**	Materials: AlN+Pt 20' AlN_Clean + 5'Pt_Clean	Materials: AlN+Pt 20' AlN_Clean + 5'Pt_Clean

		25nm AlN 30s N2/Ar 40/10sccm SP: 1500 W Bias: 6W Temp: 300° C 25 nm Pt 14s Ar 5sccm SP: 500W Bias:/ Temp:Room T	50nm AlN 1' N2/Ar 40/10sccm SP: 1500 W Bias: 6W Temp: 300° C 25 nm Pt 14s Ar 5sccm SP: 500W Bias:/ Temp:Room T
Coating Top Contact	**ACS200**	Material: AZ ECI 3007 + HDMS Thickness: 1.5 um	Material: AZ ECI 3007 + HDMS Thickness: 1.5 um
Exposure Top Contact	**Z16- MLA150**	Dose: 200mJ/cm^2 Invert Defoc -1	Dose: 210mJ/cm^2 Invert Defoc -1
Development Top Contact	**ACS200**	v	v
Inspection Top Contact	**Microscope**	v	v
Anisotropic dry etch Top Contact	**Z2 – STS**	AlN_etch: Launch 1':7'' and check the change of the color --> 1'	AlN_etch: Launch 1':10'' and check the change of the color --> 1':5''
Photoresist strip Top Contact	**Tepla Z2 or Wet Etching**	3' Strip_high	3' Strip_high
Probing electrodes	**Probe Station**	v	v
Anisotropic dry etch Top Contact	**Z2 – STS**	O2_clean 5' ALN.set 1'	ALN.set 1'40''
Photoresist strip Top Contact	**Tepla Z2**	Strip_Hight 3'	Strip_Hight 3'
Probing electrodes	**Probe Station**	v	v
Coating	**Z01- RiteTrack**	AZ ECI 3027 4um noEBR	AZ ECI 3027 4um noEBR

Release			
Exposure Release	**Z16- MLA150**	Invert Dose= 400mJ/cm2 Defoc=-2	Invert Dose=400mJ/cm2 Defoc=-2
Development Release	**Z01- RiteTrack**	v	v
Is-SiNx Etching	**SPTS**		"Si_3N_4 smooth": 2'50''
Bosch Process	**AMS**		1 chip: "SOI_accurate--": 1' 2chip: "SOI_accurate--": 1'30'' Target: 40um **Material etch rate (µm/min):3 to 4.5**
Release	**AMS**		"Si_release": 5' Target: 30um (15um per side) **Material etch rate (µm/min):≈2 in lateral**

Appendix B

Process Flow Channels

Technologies used			
DUV lithography, Dry and wet etching, RCA cleaning, LPCDV ls-SiNx deposition, SEM			
Photolithography masks			
Mask #	Critical Dimension	Critical Alignment	Remarks
1	**200 nm**	First layer	Stepper
2	**20 µm**	2um	Release
Substrate Type			
Silicon <100>, Ø100mm, 525um thick, Single Side polished, Prime, p type, 0.1-0.5 Ohm.cm Thin film : 200nm ls-SiNx.			

Step	Process description	**Cross-section after process**
A0	6'' reticle mask Fabricated externally	
01	Substrate: *Si test+ls-SiN$_x$ (200 nm)*	

02	*Photoresist coating* Material: *DUV42P + JSR KrF M35G* Machine: *ACS200* Thickness: *1200 nm*	
03	*DUV lithography + Development* Machine: *ASML PAS 5500/350c + ACS200*	
04	*Dry etching* Material: *DUV42P + ls-SiNx* Machine: *SPTS APS* Depth: *60 nm + 200 nm*	
05	*Dry Etching* Material: *Si* Machine: *AMS 200* Thickness: *6 µm*	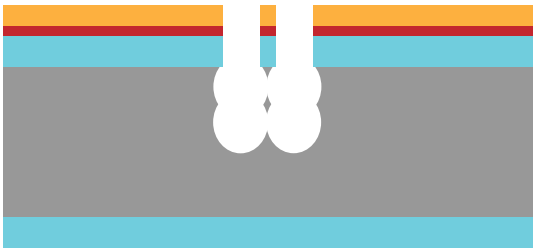
06	*PR removal* Material: *DUV42P + JSR KrF M35G* Machine: *Tepla Gigabatch*	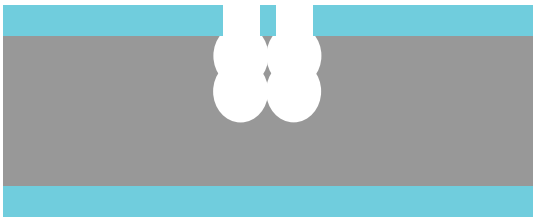
07	*Immersing to remove residues* Solution: *40% KOH* Temperature: *70°C*	

	Time: *25* Arias Base wet bench Z14	
08	*2h neutralization HCl 37%* Arias Acid wet bench Z14	
09	*SEM Inspection* Machine: *SEM Zeiss Leo*	
10	*RCA cleaning (without SRD)*	
11	*LPCVD (done by the staff, RCA)* Material: *ls* SiN_x Thickness: *300 nm*	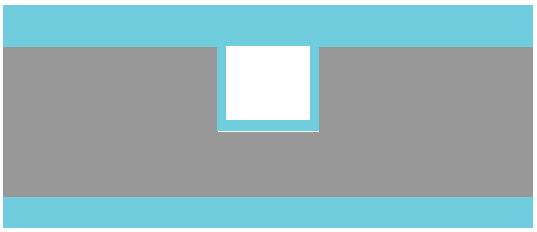

Fabrication 1

Process	Equipment	Wafer #46236 (thin PR)	Wafer #46245 (thick PR)
		Substrate: ***Si test+ls-SiN$_x$ (200 nm)***	**Substrate**: ***Si test+ls-SiN$_x$ (200 nm)***
Coating	**ACS200**	DUV42P BARC + JSR M108Y (470 nm) ACS recipe 2017	DUV42P BARC + JSR M35G (1.2 um) ACS recipe 2027
Exposure	**ASML PAS**	Nominal dose 31 mJ/cm^2 Step dose 2mJ/cm^2 Nominal focus 0 Step focus 0.3 ***The dose was stepped for each die of the grid, resulting in the top part of the wafer strongly underexposed and the bottom part strongly over-exposed.***	Nominal dose 40 mJ/cm^2 Step dose 2mJ/cm^2 Nominal focus 0 Step focus 0.3 ***The dose was stepped for each die of the grid, resulting in the top part of the wafer strongly underexposed and the bottom part strongly over-exposed.***
Development	**ACS200**	Development quickly after exposure ACS recipe 2100	Development quickly after exposure ACS recipe 2101
PR thickness measurements	**FilMetrics**	472.16 nm	1165.2nm 1146.4nm (side)
BARC etching	**SPTS**	"BARC_Slow" : 55"	"BARC_Slow" : 55"
PR thickness measurements	**FilMetrics**	372.71 nm 378.84 nm **Etching rate of PR with BARC slow : ~105nm/min**	1064.8 nm 1050.2 nm **Etching rate of PR with BARC slow : ~107nm/min**
ls-SiNx etching	**SPTS**	"Si3N4 smooth" : 1'30"	
PR thickness measurements	**FilMetrics**	287.03 nm 298.03 nm Still around 5nm of silicon nitride in the big openings (in the numbers and letters) We need to etch some more. **Etching rate of PR with Si3N4 smooth : ~55nm/min**	
ls-SiNx etching	**SPTS**	"Si3N4 smooth" : 30"	"Si3N4 smooth" : 2'
PR thickness measurements	**FilMetrics**	266.25 nm 255.48 nm	918.22 nm 924.13 nm **Etching rate of PR with BARC slow : ~68nm/min**
Si etching	**AMS200**	"Bosch SOI_accuracy" : 2'06"	"Bosch SOI_accuracy" : 2'06"

PR thickness measurements	**FilMetrics**	134.55 nm 129.80 nm **Etching rate of PR with SOI_Accu : ~61nm/min**	799.17 nm 794.98 nm **Etching rate of PR with BARC slow : ~59nm/min**
Photoresist Strip	**Tepla**	3" Strip_High There is a stain staying on the wafer. It is to be BARC according to FilMetrics	3" Strip High
PR thickness measurements	**FilMetrics**	Max 55nm BARC, shading away to ls-SiNx	583.22 nm in the center 530.54 nm on the side 373 nm at the edges **Etching rate of PR with Strip_High (center) : ~71nm/min**
Photoresist Strip	**Tepla**	4"30' Strip_High	
Inspection	**Zeiss Leo SEM**	TS0 s400g200 (under etching)	

Fabrication 2

Process	Equipment	Wafer #46239 (thin PR)	Wafer #46242(thick PR)
		Substrate: ***Si test+ls-SiN$_x$ (200 nm)***	**Substrate**: ***Si test+ls-SiN$_x$ (200 nm)***
Coating	**ACS200**	DUV42P BARC + JSR M108Y (470 nm) ACS recipe 2017	DUV42P BARC + JSR M35G (1.2 um) ACS recipe 2027
Exposure	**ASML PAS**	W=88000 h=43500 (x,y)=(0;2250) Nominal dose **31** mJ/cm^2 Step dose 2mJ/cm^2 Nominal focus 0 Step focus 0.3 NA=0.63 Sigma=0.810	W=88000 h=43500 (x,y)=(0;2250) Nominal dose **40** mJ/cm^2 Step dose 2mJ/cm^2 Nominal focus 0 Step focus 0.3 NA=0.57 Sigma=0.7
Development	**ACS200**	Development quickly after exposure ACS recipe 2100	Development quickly after exposure ACS recipe 2101
PR thickness measurements	**FilMetrics**	466.68nm	1166.1nm 1170nm
BARC+ Is-SiNx etching	**TEL**	35'' Barc + 2' Is-SiNx "CMI-BARC SiNOX"	35'' Barc + 2' Is-SiNx "CMI-BARC SiN OX"
PR thickness measurements	**FilMetrics**	163.25nm (edge)	864.08 nm (middle) 880.77 nm(center) 799.56 nm (edge)
Strip Photoresist	**TEPLA**	2'' : Strip_High	
Inspection	**SEM**	Is-SiNx well etched	Is-SiNx under etched

Fabrication 3

Process	Equipment	Wafer #46189	Wafer #46208
		Substrate: ***Si test+ls-SiN$_x$ (200 nm)***	**Substrate**: ***Si test+ls-SiN$_x$ (200 nm)***
Coating	**ACS200**	DUV42P BARC + JSR M108Y (470 nm) ACS recipe 2017	DUV42P BARC + JSR M108Y (470 nm) ACS recipe 2017
Exposure	**ASML PAS**	W=88000 h=43500 (x,y)=(0;2250) Nominal dose **31** mJ/cm^2 Nominal focus 0 NA=0.63 Sigma=0.810	W=88000 h=43500 (x,y)=(0;2250) Nominal dose **31** mJ/cm^2 Nominal focus 0 NA=0.63 Sigma=0.810
Development	**ACS200**	Development quickly after exposure ACS recipe 2100	Development quickly after exposure ACS recipe 2100
PR thickness measurements	**FilMetrics**		
BARC Etching	**TEL Or SPTS**	**35''** Barc "CMI.BARC.CF4" TEL	**55''** Barc "BARC_Slow" SPTS
PR thickness measurements	**FilMetrics**	398 nm (edges) 396.49 nm (center)	380 nm (edges) 360 nm(center)
Is-SiNx Etching	**TEL Or SPTS**	**1':30''** "CMI.SiN.OX" TEL	**2':30''** "Si3N4 smooth" SPTS
PR thickness measurements	**FilMetrics**	190 nm	180 nm
Inspection	**SEM**	S300 is well etched	S300 is not etched
Si etching	**AMS**	A)2'06'' "SOI_accurate" (7'' Etching+2'' passivation)x14cicles B)2'' "SOI_accurate++++" (8'' Etching+2''passivation)x12cycles C) 1'40'' "SOI_accurate++++" (8" Etching+2"passivation)x10cycles	
PR thickness measurements	**FilMetrics**	102nm	
Inspection	**SEM**	v	
PR strip		Acetone + IPA (we work with chips)	
	KOH +	A)--> 1',2',3',5',7',9' KOH RT A) and B) --> 20'' KOH 70°	

	HCL	C) --> 2', 3', 4' + HCL for 2h	

Fabrication 4

Process	Equipment	Wafer #88757	Wafer #88871	Wafer #88923
		Substrate: ***Si test+ls-SiN_x (200 nm)***	**Substrate**: ***Si test+lsSiN_x (200 nm)***	**Substrate**: ***Si test+ls-SiN_x (200 nm)***
Coating	**ACS200**	DUV42P BARC + JSR M108Y (470 nm) ACS recipe 2017	DUV42P BARC + JSR M108Y (470 nm) ACS recipe 2017	DUV42P BARC + JSR M108Y (470 nm) ACS recipe 2017
Exposure	**ASML PAS**	W=88000 h=43500 (x,y)=(0;2250) Nominal dose **31** mJ/cm^2 Nominal focus 0 NA=0.63 Sigma=0.810	W=88000 h=43500 (x,y)=(0;2250) Nominal dose **31** mJ/cm^2 Nominal focus 0 NA=0.63 Sigma=0.810	W=88000 h=43500 (x,y)=(0;2250) Nominal dose **31** mJ/cm^2 Nominal focus 0 NA=0.63 Sigma=0.810
Development	**ACS200**	Development quickly after exposure ACS recipe 2100	Development quickly after exposure ACS recipe 2100	Development quickly after exposure ACS recipe 2100
BARC Etching	**TEL**	**40''** Barc "CMI.BARC.CF4" TEL	**35''** Barc "CMI.BARC.CF4" TEL	**35''** Barc "CMI.BARC.CF4" TEL
ls-SiNx Etching	**TEL**	**1':40''** "CMI.SiN.OX" TEL	**1':30''** "CMI.SiN.OX" TEL	**1':30''** "CMI.SiN.OX" TEL
Si etching	**AMS**	1'40'' "SOI_accurate++++" (8"Etching+2"passivation)x 10cycles	1'40'' "SOI_accurate++++" (8"Etching+2"passivation)x 10cycles	3' "SOI_accurate++++" (8"Etching+2"passivation)x 18cycles
Photoresist Strip	**TEPLA and WET bench**	5' Strip High	1' Strip_High Wet Etching with Remover 1165: -5' Bath Remover 1165 70° -5' Bath Remover 1165 -Cascade bath H20 x3	1' Strip_High Wet Etching with Remover 1165: -5' Bath Remover 1165 70° -5' Bath Remover 1165 -Cascade bath H20 x3
BARC Strip	**TEPLA**		3' Strip_HIgh	3' Strip_HIgh
KOH	**KOH+HCL**	3' in KOH at RT+ HCL 2h	3' in KOH at RT + HCL 2h	3' in KOH at RT + HCL 2h
LPCVD			RCA cleaning Deposition of 250 um of ls-SiNx	RCA cleaning Deposition of 250 um of ls-SiNx
SEM			S300 is not open	S300 is not open